The bright end of the exo-Zodi luminosity function: disc evolution and implications for exo-Earth detectability

G. M. Kennedy[★] and M. C. Wyatt

Institute of Astronomy, University of Cambridge, Madingley Road, Cambridge CB3 0HA, UK

ABSTRACT

We present the first characterisation of the 12 μm warm dust ('exo-Zodi') luminosity function around Sun-like stars, focusing on the dustiest systems that can be identified by the *WISE* mission. We use the sample of main-sequence stars observed by *Hipparcos* within 150 pc as an unbiased sample, and report the detection of six new warm dust candidates. The ages of five of these new sources are unknown, meaning that they may be sites of terrestrial planet formation or rare analogues of other old warm dust systems. We show that the dustiest old ($>$Gyr) systems such as BD+20 307 are 1 in 10 000 occurrences. Bright warm dust is much more common around young ($<$120 Myr) systems, with a $\sim$1 per cent occurrence rate. We show that a two component in situ model, where all stars have initially massive warm discs and in which warm debris is also generated at some random time along the stars' main-sequence lifetime, perhaps due to a collision, can explain the observations. However, if all stars have only initially massive warm discs, then these would not be visible at Gyr ages, and random collisions on the main sequence are too infrequent to explain the high disc occurrence rate for young stars. That is, neither of the components can explain the observations on their own. Despite these conclusions, we cannot rule out an alternative dynamical model in which comets are scattered in from outer regions because the distribution of systems with the appropriate dynamics is unknown. Our in situ model predicts that the fraction of stars with exo-Zodi bright enough to cause problems for future exo-Earth imaging attempts is at least roughly 10 per cent, and is higher for populations of stars younger than a few Gyr. This prediction of roughly 10 per cent also applies to old stars because bright systems like BD+20 307 imply a population of fainter systems that were once bright, but are now decaying through fainter levels. Our prediction should be strongly tested by the Large Binocular Telescope Interferometer, which will provide valuable constraints and input for more detailed evolution models. A detection fraction lower than our prediction could indicate that the hot dust in systems like BD+20 307 has a cometary origin due to the quirks of the planetary dynamics. Population models of comet delivery need to be developed to help distinguish between different possible origins of warm dust.

Key words: circumstellar matter – stars: individual: HD 19257 – stars: individual: HD 23586 – stars: individual: HD 94893 – stars: individual: HD 154593 – stars: individual: HD 194931.

1 INTRODUCTION

Perhaps the most important long-term goal of humankind is to find and communicate with aliens, the inhabitants of extra-Solar systems. This goal is a difficult one, with many challenges to overcome before it is technically possible to even image an Earth-like planet around another star. When it is eventually attempted, imaging detection of these planets could still be thwarted by the presence of exo-Zodiacal (exo-Zodi) dust located in or near the terrestrial zone, which with sufficient dust levels can mask the presence of exo-Earths (e.g. Beichman et al. 2006; Absil et al. 2010; Roberge et al. 2012). Therefore, in preparation for future missions that will target specific stars, a critical piece of information is whether those stars harbour dust at a level that precludes the detection of an Earth-like planet.

While such knowledge will be crucial in specific cases, stars searched for warm dust may not be targeted in an unbiased way that yields information on the underlying distribution and its origins. For example, the most promising targets may be deemed to

★ E-mail: gkennedy@ast.cam.ac.uk

be those without cool Edgeworth–Kuiper belt analogues, or with other specific properties that may unbeknownst to us correlate with the presence of faint warm dust. The results cannot therefore be used to construct the brightness distribution (aka luminosity function, defined formally at the start of Section 3) of warm dust belts, or to make predictions for stars that were not observed or about which no dust was detected. Therefore, an equally important goal is to characterise the luminosity function, with the overall aim of understanding warm dust origin and evolution.

Evolution is of key importance here, because the brightest warm dust sources seen around nearby stars cannot necessarily maintain the same brightness indefinitely. The observed emission comes from small particles that are eventually lost from the system, and the very existence of emission for longer than terrestrial zone orbital time-scales – a few years – means that mass in small grains is being lost and replenished, and the small particles necessarily originate in a finite reservoir of larger objects. The question is whether those parent bodies are located at the same distance from the star as the dust (what we call an 'in situ' scenario) or at a much more distant location (what we call a 'comet delivery' scenario).

The possibility of such different origins means that the rate at which warm dust decays is unknown. For example, if the observed dust has its origins in an outer Edgeworth–Kuiper belt analogue and is scattered inward by planets (i.e. a comet delivery scenario; Nesvorný et al. 2010; Bonsor & Wyatt 2012; Bonsor, Augereau & Thébault 2012), the warm dust could be extremely long lived. Given the lack of evolution seen for main-sequence exo-Kuiper belts around Sun-like stars (e.g. Trilling et al. 2008), dust levels may not appear to decay at all during the stellar main-sequence lifetime. If, however, the dust originates near where it is observed (i.e. in situ), it would decay due to a decreasing number of parent bodies via collisions in a way that is reasonably well understood (e.g. Dominik & Decin 2003; Wyatt et al. 2007a; Löhne, Krivov & Rodmann 2008). In this scenario, it also follows that the brightest warm discs are necessarily the tip of an iceberg of fainter discs; the decay time-scale depends on the amount of mass that is present so systems decay as 1/time (e.g. Dominik & Decin 2003), and for every detection of bright warm dust that was created relatively recently, many more exist that are older and fainter, and are slowly grinding themselves to oblivion. Another conclusion from this kind of evolution is that the bright warm dust systems seen around relatively old stars cannot arise from in situ decay that started when the star was born; projecting the 1/time decay back to early times predicts implausibly large initial brightnesses, and delaying the onset of this decay for ~Gyr time-scales within a steady-state scenario requires implausibly large or strong planetesimals (Wyatt et al. 2007a).

These two different origins present very different structural and dynamical pictures of planetary systems, which may manifest differently in the warm dust luminosity function. For example, an observed luminosity function similar to that expected from 1/time decay would be a smoking gun for in situ origin and evolution. However, because the luminosity function in the comet delivery scenario is at least in part set by the (unknown) distribution of systems with the appropriate structural and dynamical properties, and the source regions may themselves be decaying as 1/time, the observation of such a function would not be absolute proof. As a further complication, it may be that the processes that generated the dust in BD+20 307 and HD 69830 systems (i.e. the dustiest warm systems, whose host stars are ~Gyr old) are completely different to those that result in the faintest systems. It could for example be that BD+20 307-like systems are the result of late (i.e. ~Gyr) dynamical instabilities

(Song et al. 2005), while faint Asteroid belt and Zodiacal cloud-like systems are the decay products of young massive belts that emerged from the protoplanetary disc phase or arise due to comet delivery. Therefore, our work here must be complemented by studies that, for example, aim to discover whether warm dust is correlated with the presence of cooler dust (e.g. Absil et al. 2013).

Here, we use the stars observed by *Hipparcos* (van Leeuwen 2007) as an unbiased sample to characterise the bright end of the warm dust luminosity function using mid-infrared (IR) photometry from the *WISE* mission (Wright et al. 2010). A secondary goal is to discover new bright warm discs, though few discoveries are expected among these stars due to previous *IRAS* and AKARI studies with a similar goal (e.g. Aumann & Probst 1991; Oudmaijer et al. 1992; Song et al. 2005; Fujiwara et al. 2010, 2012a; Melis et al. 2012). The key difference between those studies and ours is that we count the non-detections, and therefore quantify the rarity of bright warm dust systems. We first outline our sample (Section 2) and excess (Section 3) selection, and then cull disc candidates from these excesses (Section 4). We go on to compare the luminosity function with a simple in situ evolutionary model and make some basic predictions within the context of this model for future surveys for faint warm dust (Section 5). Finally, we discuss some of the issues with our model and comet delivery as an alternative (but equally plausible) exo-Zodi origin (Section 6).

2 SAMPLE DEFINITION

Stars are selected from the *Hipparcos* catalogue (van Leeuwen 2007) using an observational Hertzsprung-Russell (HR) diagram. Because warm dust and planets have been discovered over a wide range of spectral types that might be taken as 'Sun-like', we use a fairly broad definition of $0.3 < B_T - V_T < 1.5$, in addition only keeping stars with $B_T < 11$ to ensure that the Tycho-2 photometric uncertainties are not too large (Høg et al. 2000), particularly for faint cool M types and white dwarves that otherwise creep into the sample. Using the Tycho-2 Spectral Type Catalogue (Wright et al. 2003), the main-sequence spectral types whose most common $B_T - V_T$ colours are 0.3 and 1.5 are A8 and K5, respectively. While stars have a range of colours at a given spectral type, the bulk of the spectral types in our sample will lie between these bounds. To ensure that we do not select heavily reddened or evolved stars that are wrongly positioned in the HR diagram, we only retain stars within 150 pc, and restrict the parallax signal to noise ratio (S/N) of stars to be better than 5. Finally, we exclude stars within 2° of the Galactic plane, as we found that many *WISE* source extractions, even for relatively bright stars, are unreliable there. With these cuts 27 333 stars remain.

We exclude evolved stars, which may show excesses due to circumstellar material associated with mass-loss, by excluding stars with $M_{H_p} > 5$ when $B_T - V_T > 1.1$, and with $M_{H_p} > 25/3(B_T - V_T - 0.5)$ when $B_T - V_T \leq 1.1$ (3159 stars).[1] This cut is based purely on by-eye inspection of Fig. 1, but as long as it lies in the Hertzsprung gap the sample size is only weakly sensitive to actual position because there are few stars there. The line is broken at 1.1 because a single line does not simultaneously exclude most stars crossing the Hertzsprung gap and include pre-main-sequence stars such as HD 98800 (the rightmost filled circle at $B_T - V_T = 1.4$,

---

[1] H_p is a *Hipparcos*-specific bandpass, whose response peaks at about 5000 Å with a full width at half-maximum sensitivity of about 2000 Å. See Bessell (2005) for a comparison with other passbands.
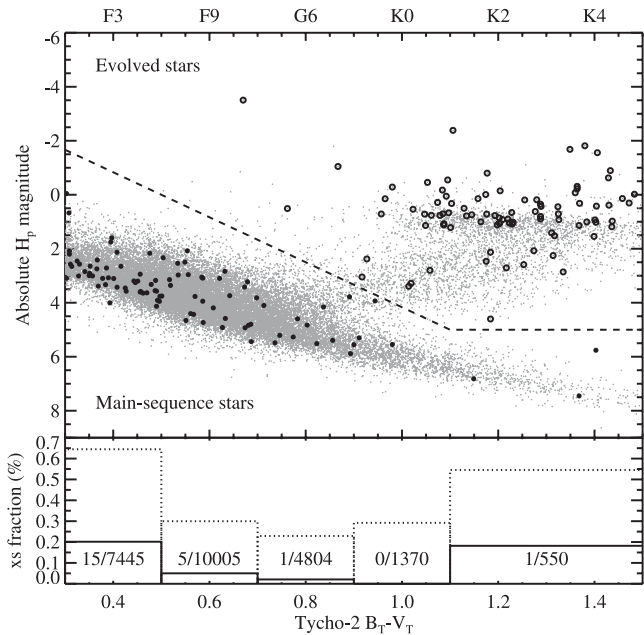
Figure 1. Top: HR diagram showing stars with $0.3 < B_T − V_T < 1.5$, split into Sun-like main-sequence stars and evolved stars by the dashed line. The top axis shows spectral types calculated using synthetic photometry of PHOENIX stellar atmosphere models (Brott & Hauschildt 2005). Stars with $W1 − W3$ greater than 0.1 mag are shown as circles: open for evolved stars and filled for main-sequence stars. Bottom: fraction of main-sequence stars with $W1 − W3 > 0.1$. The dotted bars show all stars with $W1 − W3 > 0.1$ (i.e. filled dots in the top panel), while the solid bars and numbers show those with plausible warm dust emission after individual checking (see Section 4).

$H_p = 6$). Because they are selected solely using optical photometry and parallax, the 24 174 stars selected by these criteria are unbiased with respect to the presence of warm dust. The *Hipparcos* HR diagram for the sample is shown in Fig. 1, which shows all 27 333 stars within the $B_T − V_T$ range, the cut used to exclude evolved stars (dashed line), and those found to have 12 μm excesses by the criteria described below (large dots and circles).

2.1 Age distribution

It will become clear later that knowing the age distribution of our sample stars is useful. The simplest assumption would be that the ages are uniformly distributed. However, given the tendency for stars to have earlier types than the Sun (Fig. 1), this assumption yields an unrealistically high fraction of ~10 Gyr old main-sequence stars (i.e. spectral types later than the Sun). Our sample spans a sufficiently wide range of spectral types that the main-sequence lifetimes vary significantly. For example, the earliest spectral types are late A-types, with ~Gyr main-sequence lifetimes, while the latest spectral types are late K-types, with main-sequence lifetimes exceeding the age of the Universe. Stars are therefore assumed to have ages distributed uniformly between zero and their spectral-type-dependent main-sequence lifetime, with the overall age distribution derived using the distribution of $B_T − V_T$ colours (i.e. the colours are used as a proxy for the distribution of spectral types, a full description is given in Appendix B). The final age distribution is shown in Fig. 2, which we assume throughout. Using a more simplistic assumption of uniformly distributed ages between 0 and 10 Gyr for all stars does not alter any of our conclusions.
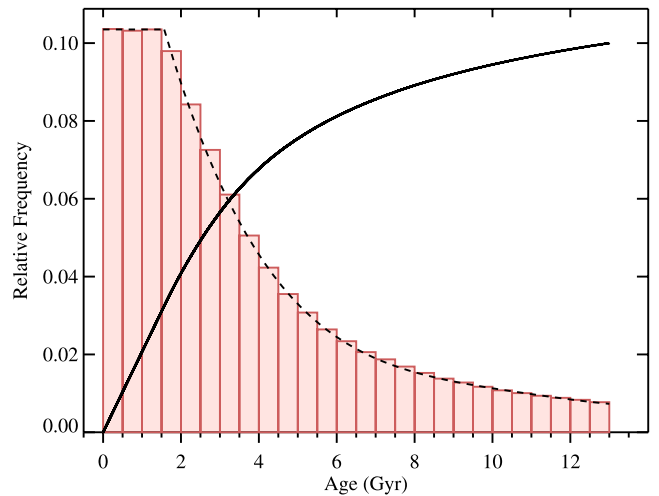
Figure 2. Spectral type-weighted age distribution adopted for our sample. The line shows the cumulative fraction (divided by 10). Thus, about 50 per cent of our stars are younger than 2.5 Gyr. The dashed line shows the constant relative frequency of 0.1035 and the fourth-order polynomial fit used to generate synthetic age populations (see Appendix B).

3 EXCESS SELECTION

If warm dust is sufficiently bright relative to the host star, it will manifest as a detectable mid-IR (i.e. 10–20 μm) excess relative to the stellar photosphere, which for ~300 K dust peaks near 12 μm. The *WISE* bands are well suited for this task, and because it has about an order of magnitude better sensitivity to 300 K dust compared to W4 (see fig. 2 of Kennedy & Wyatt 2012) we use the 12 μm $W3$ band.[2]

Our luminosity function is therefore formally the distribution of 12 μm disc-to-star flux density ratios, which we will use in cumulative form. We use the term 'luminosity function' largely for conciseness. The disc luminosity of course not only depends on the 12 μm flux ratio, but also on the disc temperature and stellar properties. If the ratio of the observed to stellar photospheric flux density is $R_{12} = F_{12}/F_\star$, and the disc-to-star flux ratio is $\xi_{12} = R_{12} − 1$, then the luminosity function is the fraction of stars with ξ_{12} above some level.

To derive the 12 μm luminosity function, we would ideally have a sample for which the sensitivity to these excesses is the same for all stars. Then the distribution is simply the cumulative excess counts divided by the total sample size. Our use of *Hipparcos* stars with the above parallax requirement ensures that this ideal is met; all stars in our overall sample have better than 6 per cent photometry at 1σ in $W3$, and 98 per cent have better than 2.5 per cent photometry at 1σ. Given that the calibration uncertainty in this band is 4.5 per cent (Jarrett et al. 2011), the fractional photometric sensitivity for all sample stars is essentially the same at about 5 per cent 1σ. Therefore, the disc sensitivity is 'calibration limited' for our purposes (see Wyatt 2008), with a 5 per cent contribution from the *WISE* photometry, and a ~2 per cent contribution from the stellar photosphere. That is, we are limited to finding 3σ 12 μm excesses brighter than about 15 per cent of the photospheric level (flux ratios of $R_{12} \geq 1.15$). This property means that we can select excesses by choosing stars with a red 3.4−12 μm ($W1 − W3$) colour.

---

[2] The *WISE* bands are known as $W1$, $W2$, $W3$ and $W4$, with wavelengths of 3.4, 4.6, 12 and 22 μm, respectively (Wright et al. 2010; Jarrett et al. 2011).
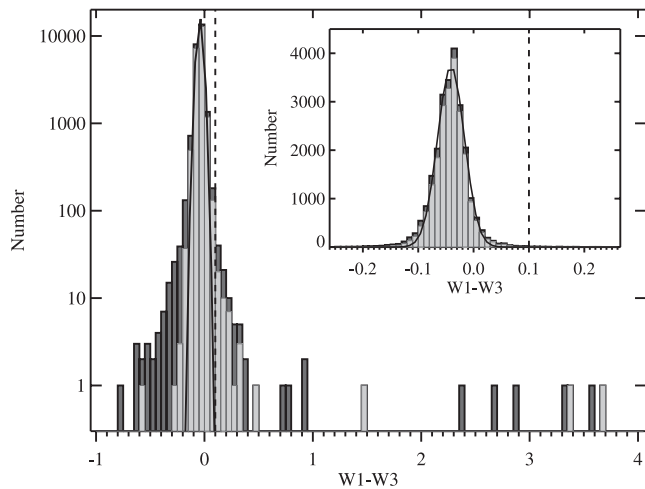
Figure 3. Histograms of $W1 - W3$ colours for 24 174 main-sequence stars (i.e. those below the dashed line in Fig. 1). The inset shows a smaller range of $W1 - W3$ with a linear count scale. The dark grey bars show all sources and light grey bars show only sources where the *WISE* extension flag is not set (i.e. ext_flg=0). Curves show Gaussian fits to the overall sample. The dashed line shows the threshold of $W1 - W3 = 0.1$ mag for stars to become excess candidates (filled dots in Fig. 1).

Though our excess limit is a uniform 15 per cent due to the sample stars being bright, this brightness brings other potential problems. Stars brighter than 8.1, 6.7, 3.8 and −0.4 mag are saturated in $W1 - 4$, respectively, so nearly all stars are saturated in the W1 band to some degree, while only about a hundred are saturated in W3. However, comparison with Two Micron All Sky Survey (2MASS) photometry shows that the *WISE* W1 source extraction is reliable well beyond saturation and shows no biases up to about 4.5 mag, and only about 400 stars are brighter than this level.[3] Therefore, saturation actually affects a very small fraction of our stars. However, bright stars are the nearest to Earth and therefore potentially important for future studies if warm dust can be discovered, so we need to be sure that we are not biased against true excesses, i.e. that excesses selected based on $W1 - W3$ are not systematically missed due to some problem associated with W3. We did not find any signs of W3-specific issues, but noted that the S/N of W1 photometry depends fairly strongly on stellar brightness, with the brightest (i.e. more saturated) stars having lower S/N (i.e. stars brighter than about 7.25 mag in V_T have S/N < 20). The increased $W1 - W3$ scatter for these stars means some excesses may be missed for those with W1 that happens to be scattered brighter than the actual brightness. This issue affects ∼1000 stars, and we show in Section 4.4 that we can rule out missing excesses for the worst of these cases. Given that there is no evidence for a problem with using $W1 - W3$ to identify excesses, we now proceed and leave possible issues with the *WISE* photometry to be identified in the individual source checking stage below.

The $W1 - W3$ distribution of the 24 174 stars is shown in Fig. 3. A Gaussian fit centred on $W1 - W3 = -0.041$ with dispersion $\sigma = 0.024$ is shown, the fit being consistent with the photometric accuracy described above. The slightly negative average colour arises because our stars are later spectral types than the reference A0V spectrum used for Vega magnitudes. The logarithmic scale (main plot) shows that systematic effects spread the distribution further for

a relatively small number of sources. We therefore looked for properties that appear to predict $W1 - W3$ colours significantly different to −0.041 as indicators of systematic effects. Stars with companion sources at separations of 5–16 arcsec in the *Hipparcos* catalogue are more likely to have $W1 - W3 < 0.3$, as are *WISE*-saturated sources. We found that the best indicator of negative $W1 - W3$ was the *WISE* extension flag (ext_flg), which indicates sources not well described by the *WISE* point spread function, or those near extended sources in the 2MASS Extended Source Catalogue. Aside from a few very bright sources, there is little brightness dependence on $W1 - W3$ colour, so it seems that the bulk of sources with blue *WISE* colours are due to poor source extractions for confused sources. Five of the warm dust candidates found below have ext_flg = 1, but four are already known to host warm dust. For this reason, and because we subsequently check them individually we cull candidates from the full list of 24 174 stars.

The *WISE* W3 calibration-limited sensitivity of about 5 per cent, combined with the average $W1 - W3$ colour of −0.04 means that a sensible threshold to use for true 12 μm excesses that can be found to be significant is about 0.1 mag. While we could choose a slightly lower threshold to include more sources that may turn out to be robust after more detailed analysis, this threshold is also practical in that it limits the number of sources to check by hand to a reasonable number; as we show below the false-positive rate already is fairly high and we expect this rate to increase strongly as the threshold moves closer to −0.04 (e.g. decreasing the threshold from 0.15 to 0.1 roughly doubles the number of sources to check, but only results in 25 per cent more warm dust candidates, and decreasing the threshold to 0.05 would yield 181 more sources to check). Stars later than about K0 have slightly redder $W1 - W3$ than average (tending to about zero colour for $B_T - V_T = 1.5$). This trend has the potential to add more false positives, but in practise does not because it only affects a few hundred stars. We therefore identify as promising 12 μm excess candidates the 96 main-sequence stars with $W1 - W3$ above 0.1, which are marked as large filled dots in Fig. 1. Stars this red may show a 3σ W3 excess based on the photometric uncertainties of most stars. To study these 96 sources further we use χ^2 minimization to fit PHOENIX stellar photosphere (spectral energy distribution, SED) models (Brott & Hauschildt 2005) to 2MASS, *Hipparcos* (Perryman & ESA 1997), Tycho-2 (Høg et al. 2000), AKARI (Ishihara et al. 2010) and *WISE* $W1-2$ photometry (Wright et al. 2010) to provide a more accurate prediction of the W3 flux density to compare with the *WISE* measurements. The SED fitting method has previously been validated through work done for the *Herschel* DEBRIS survey (e.g. Kennedy et al. 2012a,b)

4 WARM DUST CANDIDATES

We now check the 96 stars with candidate excesses for plausibility by inspecting the SEDs and *WISE* images for each source. The issues that arise are all due to *WISE* source extraction, but for several different reasons. Some are affected by bright nearby sources and image artefacts, while others are moderately separated binary systems where the *WISE* source extraction has only measured a single source. In some cases, the W1 photometry is shown to be underestimated, generally due to saturation. The results of the SED fitting alone are not sufficient for recognizing spurious excesses and image inspection is generally required. While we inspected all of the images for the few candidates identified here, there are commonly indications in the *WISE* catalogue – primarily apparent variability – that might be used in a larger study. Notes on individual sources are given in Appendix A. We find 25 systems with plausible and

[3] http://wise2.ipac.caltech.edu/docs/release/allsky/expsup/sec6_3c.html

Table 1. Significant 12 μm excess candidates, new excesses are marked with a *. $T_{\rm BB}$ is the blackbody temperature fitted to the warm dust emission (in K). See Appendix A for notes on all 96 sources considered. Spectral types are from SIMBAD. References: 1: Zuckerman et al. (2008), 2: Weinberger et al. (2011), 3: Fujiwara et al. (2012b), 4: Fujiwara et al. (2012a), 5: Melis et al. (2010), 6: Sierchio et al. (2010), 7: Mamajek (2005), 8: de Zeeuw et al. (1999), 9: Chen et al. (2012), 10: Oudmaijer et al. (1992), 11: Zuckerman & Becklin (1993), 12: Yang et al. (2012), 13: Chen et al. (2011), 14: Smith, Wyatt & Haniff (2012), 15: Rizzuto, Ireland & Robertson (2011), 16: Carpenter et al. (2009), 17: Honda et al. (2004), 18: Gregorio-Hetem et al. (1992), 19: Fajardo-Acosta, Beichman & Cutri (2000), 20: Holmberg, Nordström & Andersen (2009), 21: Rizzuto, Ireland & Zucker (2012) and 22: Tetzlaff, Neuhäuser & Hohle (2011).

HIP	Name	R_{12}	$T_{\rm BB}$	Spty	Age	Group	Comments
8920	BD+20 307	27.4	440	G0	~1 Gyr		Close binary, no cold dust. (1, 2)
11696	HD 15407A	5.4	560	F5	80 Myr		No cold dust. (3, 4, 5)
*14479	HD 19257	2.1	250	A5	?		
17091	HD 22680	1.2	200	G	115 Myr	Pleiades	(6)
17401	HD 23157	1.2	180	A5	115 Myr	Pleiades	(6)
*17657	HD 23586	1.4	290	F0	?		
*53484	HD 94893	1.2	150	F0	?	LCC?	Membership uncertain. (7)
56354	HD 100453	91.6	–	A9	17 Myr	LCC	Herbig Ae. (8, 9, 10)
55505	HD 98800B	7.6	170	K4	8 Myr	TWA	Close binary in quadruple system. Possible transition disc. (11, 12)
58220	HD 103703	1.4	260	F3	17 Myr	LCC	(8, 13)
59693	HD 106389	1.3	290	F6	17 Myr	LCC	(8, 13)
61049	HD 108857	1.4	230	F7	17 Myr	LCC	(8, 13)
63975	HD 113766A	1.4	300	F4	17 Myr	LCC	Excess around primary in 160 au binary. (8, 14)
64837	HD 115371	1.2	238	F3	17 Myr	LCC	Membership probability 50 per cent. (15)
73990	HD 133803	1.2	180	A9	15 Myr	UCL	(8, 9)
78996	HD 144587	1.4	220	A9	11 Myr	US	(8, 16)
79288	HD 145263	13.6	240	F0	11 Myr	US	(8, 9, 17)
79383	HD 145504	1.2	206	F0	17 Myr	US	(15)
79476	HD 145718	110.0	–	A8	17 Myr	US	Herbig Ae. (8, 18)
81870	HD 150697	1.2	234	F3	3.2 Gyr?	?	Near edge of ρ Oph star-forming region so may be younger. (19, 20)
*83877	HD 154593	1.2	285	G6	?		
86853	HD 160959	1.6	210	F0	15 Myr?	UCL?	Membership probability 50 per cent due to excess (21), may be older (20)
*88692	HD 165439	1.2	200	A2	11 Myr?		Age uncertain? (22)
89046	HD 166191	45.9	?	F4	?		Protoplanetary disc? (suggests young age)
*100464	HD 194931	1.2	188	F0	?		

significant 12 μm excesses, of which all but six were previously known to host significant levels of warm dust. These six should be considered as promising candidates and require further characterisation, but are considered here to be real. The 25 are listed in Table 1 and detailed SEDs are shown in Appendix C.

The inclusion or exclusion of targets from the list of 25 in the context of our goal here merits some discussion. Because we wish to find the warm dust luminosity function for main-sequence stars, our sample should include any object that plausibly looks like a debris disc, even if it appears to be an extreme specimen. Though the most extreme discs, such as BD+20 307 are very rare, this rarity is unsurprising, at least in an in situ scenario; brighter (i.e. more massive) discs decay more rapidly due to more frequent collisions, resulting in a decreased detection probability at the peak of their activity.

4.1 Protoplanetary discs

We do not include protoplanetary discs in our luminosity function because they represent a qualitatively different phase of evolution to the debris disc phase (e.g., models of their decay are not simply power laws; Clarke, Gendrin & Sotomayor 2001). Including protoplanetary discs would require that models of the luminosity function include a prescription for the poorly understood transition from this phase to the debris disc phase, which would be very uncertain and limit our interpretation.

In terms of photometry the main feature that distinguishes protoplanetary discs from debris discs is the breadth of the disc emission spectrum. Protoplanetary discs cover a wide range of radii and extend right down to near the stellar surface, and therefore have near-, mid- and far-IR excesses. On the other hand, debris discs are usually well described by blackbodies, sometimes with the addition of spectral features. In some cases (e.g. η Corvi, HD 113766A; Sheret, Dent & Wyatt 2004; Wyatt et al. 2005; Morales et al. 2011; Olofsson et al. 2013), debris discs are poorly fitted by a single temperature component, suggesting that populations of both warm and cool dust exist, and may argue for a comet delivery scenario for the warm dust with the cool component acting as the comet reservoir (Bonsor & Wyatt 2012). These systems are however easily distinguished from protoplanetary discs because the cool debris disc components always have much lower fractional luminosities than protoplanetary discs ($L_{\rm disc}/L_\star \lesssim 10^{-4}$ compared to $\sim 10^{-1}$; e.g. Trilling et al. 2008).

A more useful discriminant for our purposes is that debris discs never have large near-IR excesses. This lack of near-IR emission is first seen as the protoplanetary disc is dispersed in so-called transition discs (Skrutskie et al. 1990). We therefore formalize the protoplanetary–debris disc distinction by considering the presence of a near-IR (3.4 μm) excess, using the $K_{\rm s} - W1$ colour. While all sources were selected to have a red $W1 - W3$ colour, the addition of a sufficiently large $W1$ excess indicates that the source is probably a protoplanetary disc. The $K_{\rm s} - W1$ colours for the sources in Table 1 are all less than 0.2, with three notable exceptions. The first two are the Herbig Ae stars HD 100453 and HD 145718 ($K_{\rm s} - W1 \approx 0.9$), and the third is a new potential warm dust source, HD 166191 ($K_{\rm s} - W1 = 0.5$), which we discuss further below. The SEDs of all three

are shown in Appendix C, and with both near and far-IR excesses are clearly different from the other 22. The detection of significant far-IR excesses by *IRAS* indicates emission from cold material but we did not use this as a discriminant because it would not have been detectable around all sources, even if a protoplanetary disc was present.

HD 166191 has only recently been noted as a potential warm dust source (Fujiwara et al. 2013), though was reported as having an IR excess from both *IRAS* and MSX (Oudmaijer et al. 1992; Clarke, Oudmaijer & Lumsden 2005).[4] In addition, an excess was detected with the AKARI Infrared Camera (IRC) at 9 and 18 μm, but not with the AKARI Far-Infrared Surveyor (FIS) from 65–160 μm (though the upper limit from AKARI-FIS is about 10 Jy, so not strongly constraining). An excess was found in the *IRAS* 60 μm band, suggesting that the excess emission extends into the far-IR. A large excess over a wide range of IR wavelengths suggests that the emission is at a wide range of temperatures, and therefore that HD 166191 in fact harbours a protoplanetary disc. However, a nearby (1.7 arcmin) red source was detected by *WISE*, MSX and AKARI-IRC, opening the possibility that because *IRAS* had poor resolution the far-IR emission in fact comes from the nearby source and not HD 166191. A preliminary conclusion from new *Hershel* Photodetector Array Camera and Spectrometer (PACS, Pilbratt et al. 2010; Poglitsch et al. 2010) observations is that the disc spectrum is more consistent with a protoplanetary disc; given the *WISE* photometry, both the 70 μm flux density ($\approx$1.7Jy) and the fractional luminosity ($\approx$10 per cent) are larger than would be expected for a warm debris disc. A detailed study of this source will be presented elsewhere.

Finally, though it is not excluded by its $K_s - W1$ colour, HD 98800 merits some discussion because whether it is a young debris disc or in the transition between the protoplanetary and debris disc phases is unclear. The disc emission spectrum is well modelled by a blackbody, as are most debris discs. The fractional luminosity is very high at around 10 per cent, meaning that a significant fraction of the star's emission is being reprocessed by the disc. However, the far-IR emission may be decreased compared to that expected from a protoplanetary disc by truncation by the outer binary (Andrews et al. 2010). In addition, the detection of H_2 emission suggests that HD 98800 may still harbour some circumstellar gas (Yang et al. 2012), though CO emission has not been detected (Zuckerman, Forveille & Kastner 1995; Andrews et al. 2010). Based on the age, blackbody-like emission, and lack of CO detection and near-IR excess we include HD 98800 in our luminosity function, with the expectation that it will decay in a deterministic manner and that it is therefore both a plausible warm dust source and direct progenitor of fainter warm dust systems.

4.2 Warm debris discs

Having excluded three sources from the original list of 25, we now consider some properties of the remaining 22. For each source, after fitting a stellar photosphere model we fit a blackbody disc model to any significant IR excesses. In general, blackbody models are a reasonable match to debris disc emission, though the agreement is poorest for warm dust systems, which commonly have non-continuum silicate features (e.g. Song et al. 2005; Fujiwara et al. 2010). However, the temperatures derived are representative,

---

[4] None of the other new disc candidates were detected by *IRAS*, but see Appendix A notes for HIP 14479.

and more complicated models are unwarranted because we typically only have 2 to 3 data points to fit.[5]

The warm dust sources have a range of temperatures, which correspond to a range of radial distances. While we are not explicitly looking for habitable-zone dust, it is instructive to compare the temperatures to the width of the 'habitable zone', which is naively the radial distance at which the equilibrium temperature is $\sim$280 K (i.e. the temperature of a blackbody at 1 au from the Sun). The width of the habitable zone is of course very uncertain, and is probably at least a factor of 2 wide in radius (Kasting, Whitmire & Reynolds 1993; Kopparapu et al. 2013). Therefore, the temperature range allowed is at least a factor of $\sqrt{2}$ wide, giving a range from approximately 230 to 320 K. In addition, there is considerable uncertainty in the location of dust belts inferred from SED models for several reasons, such as the likely presence of non-continuum spectral features [e.g. all warm dust targets considered transient by Wyatt et al. (2007a) have silicate features]. In addition, belts may be a factor of $\sim$2 more distant than inferred from blackbody models due to grain emission inefficiencies at long wavelengths (relative to their sizes; e.g. Booth et al. 2013). However, this factor, which has been derived from cool Kuiper belt analogues, may not apply to fainter warm dust if larger grains dominate the emission. Finally, the picture of a ring of warm dust is probably oversimplified, particularly at faint levels where Poynting–Robertson drag becomes important. Based on this discussion, we retain all 12 μm excess sources in what follows. In any case, removal of the coolest few sources (those below 200 K say) would make little difference to our analysis. Temperature is of course worthy of future study, and for example the luminosity function could (with sufficient detections) be extended to include it as a third dimension.

It is clear from Table 1 that the 12 μm excess systems are preferentially young, with at least 11 (and possibly 13) being members of the Scorpius–Centaurus association in Lower Centaurus Crux (LCC), Upper Centaurus Lupus (UCL) and Upper Scorpius (US) (i.e. <20 Myr old). In addition, HD 98800 belongs to the 8 Myr old TW Hydrae association (TWA), HD 165439 was derived to be 11 Myr based on isochrone models (Tetzlaff et al. 2011), HD 15407A is a member of the AB Doradus moving group (Melis et al. 2010), and HD 22680 and HD 23157 belong to the 115 Myr old Pleiades. Of the seven stars that are not known to be young, only BD+20 307 is known to be older than about 1 Gyr. HD 160959 was suggested to be a member of UCL with 50 per cent probability (i.e. 15 Myr old; Rizzuto et al. 2012), but also has an isochrone-derived age of 1.4 Gyr (Holmberg et al. 2009). Based on the likelihood of stars with excesses to be young, the former age seems more likely to be correct, but merits further study. Similarly, HD 150697 is suggested to be 3.2 Gyr old based on isochrones (Holmberg et al. 2009), but with a similar sky location and distance as the ρ Ophiuchi starforming region (Fajardo-Acosta et al. 2000) requires further study to verify the age.

For a typical main-sequence lifetime of 10 Gyr and stars spaced randomly throughout, there is a 1 per cent chance of a star being randomly younger than 100 Myr. However, 15 (possibly 18) of the 22 systems are younger than 120 Myr, implying that the warm disc occurrence rate for stars this young is at least 5 per cent. Therefore, as with longer wavelengths (i.e. 24 μm; Siegler et al. 2007),

---

[5] We use a 'modified' blackbody, where the emission beyond $\lambda_0 = 210$ μm is multiplied by λ_0/λ (see Wyatt 2008) to account for inefficient emission from small grains. While this modification is not needed, it ensures that submillimetre fluxes predicted by the models are more realistic than a pure blackbody.

there appears to be a significant decrease in the incidence of 12 μm emission with time. However, this decay is unlikely to be universal; BD+20 307 is at least 1 Gyr old, so assuming 1/time ($1/t$) decay should have been ∼100 times brighter at 10 Myr (i.e. verging on physically impossible given that the fraction of the host star's light that is captured by the dust is currently 3.2 per cent; Weinberger et al. 2011). Therefore, the more reasonable conclusion is that either the dust level in this system is not evolving, as might be expected in a comet delivery scenario, or became very bright some time well after the protoplanetary disc was dispersed, as might be expected for a recent collision.

The stars in Table 1 are biased towards earlier spectral types, though the histogram in Fig. 1 shows that this could be explained by more early-type stars in the sample distribution. Based on the histogram there is some evidence that earlier spectral types are more likely to host 12 μm excesses. The likely explanation is that later type stars in the sample are biased somewhat against having younger ages, as it is only the brighter (earlier type) stars in the nearby young associations that were selected for the *Hipparcos* sample.

4.3 Variability

Given the possibly transient nature of warm dust, particularly in old systems such as BD+20 307, we made a basic search for variability using the *WISE* data. This search is motivated by the likely orbital time-scales being of the order of years, and the ability of individual collisions to affect the overall dust level (Kenyon & Bromley 2005; Wyatt et al. 2007a; Meng et al. 2012). Indeed, evidence for ∼year time-scale variability has been seen in several relatively young warm dust systems (Melis et al. 2012; Meng et al. 2012).

Though stars were only observed over a day or so in a single *WISE* pass, another was made six months later for sources that were in the appropriate RA range.[6] Of the 22 warm dust sources, only BD+20 307 and HD 103703 show evidence for *WISE* variability. HD 103703 is marked as variable in *W3* in but not W4. While it may be possible for *W3* to vary while W4 stays constant due to changes in the strength of silicate features or the emission from each being dominated by emission at different radial dust locations, the change of ∼0.1 mag (±0.02 mag) in only one band is suggestive but requires verification. In contrast, BD+20 307 shows a brightening of 6–8 per cent in both *W3* and W4 over a six month period (see also Meng et al. 2012), and as shown in Fig. 4, these are correlated in the sense that an increase in *W3* brightness is accompanied by an increase at W4. This increase suggests that while the total mass (i.e. including parent bodies) must be decreasing (or at least be constant), effects such as individual collisions, size distribution variations and mineralogical changes can increase the amount of dust as measured by the IR excess on ∼year long time-scales.

4.4 Missing warm dust sources?

An apparent omission from our warm dust list is HD 69830. As one of the nearest few dozen Sun-like stars and host to both planets and warm dust, it is of key importance (Beichman et al. 2005). The reason it does not appear here is in fact simple; the excess at 12 μm is not large enough to be formally detected with *WISE*. A detailed SED model that includes all available photometry, including that
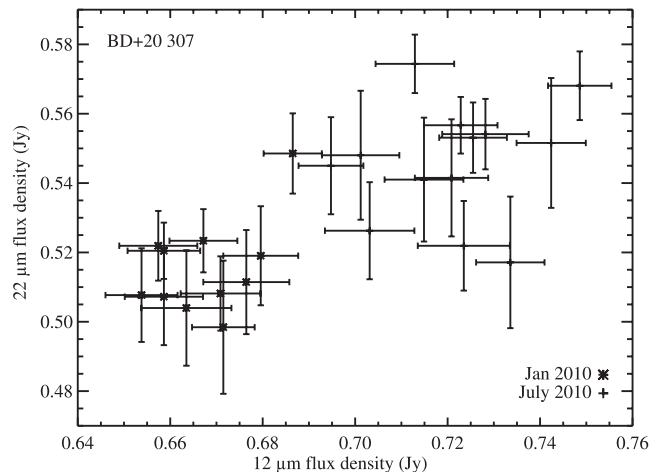
Figure 4. Evidence for a positive increase in the BD+20 307 mid-IR emission from 2010 January 19 to July 26. Data are from the *WISE* single exposure catalogue and exclude the last image from each period, which have clear artefacts.
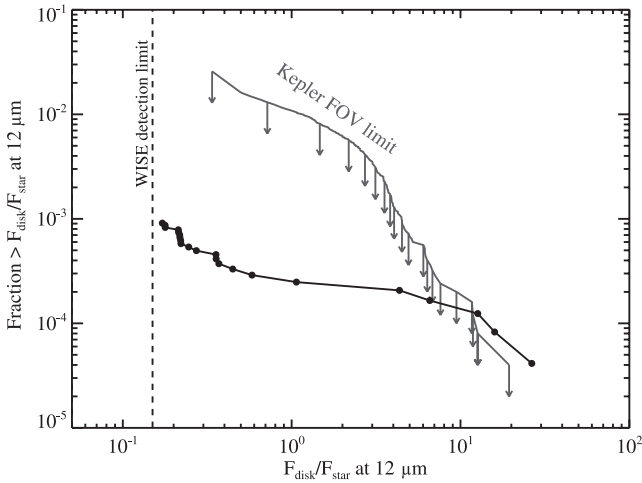
from the *Spitzer* Infrared Array Camera (Fazio et al. 2004; Werner et al. 2004), shows that the 12 μm excess is only at the 5 per cent level, which also agrees with *IRAS* (see also fig. 2 in Beichman et al. 2011). Another key warm dust source is the F2V star η Corvi, which has $W1 - W3$ of 0.14 and a *W3* excess significance of only $2σ$. The 'disappearing disc' TYC 8241-2652-1 (Melis et al. 2012) is not included here because it is not in the *Hipparcos* catalogue. Similarly, well known A-type warm dust sources such as β Pictoris and HD 172555 have significant *WISE* 12 μm excesses, but with $B_T - V_T$ colours of around 0.2 were not part of the initial sample.

We made a further check for potential warm dust sources within the Unbiased Nearby Stars (UNS) sample, which includes five samples, each having the nearest ∼125 main-sequence stars with spectral types of A, F, G, K and M (i.e. 125 A stars, 125 F stars, etc.; Phillips et al. 2010). UNS stars meeting the criteria outlined above are a subset of the larger sample in question here, and SEDs for this sample have been studied in great detail as part of the *Herschel* DEBRIS Key Programme (e.g. Kennedy et al. 2012a; Wyatt et al. 2012). With the inclusion of *IRAS* (Moshir et al. 1993) and AKARI (Ishihara et al. 2010) mid-IR photometry, and in many cases *Spitzer* Infrared Spectrograph (IRS; Houck et al. 2004; Lebouteiller et al. 2011) spectra, this subset therefore provides a good check for the sources that are subject to the worst saturation effects. We found no 12 μm excesses in this subset that should have resulted in a significant detection with *WISE*.

4.5 The 12 μm luminosity function

Fig. 5 shows the 12 μm luminosity function that results from the 22 unbiased warm dust detections described above. The distribution is generated simply by assuming that these excesses could have been detected around all 24 174 stars, and dividing the cumulative disc-to-star flux ratio distribution by this number. Thus, while the brightest warm dust systems such as BD+20 307 are known to be rare, we have quantified this rarity to be of the order of 1 in 10 000.

Fig. 5 also compares the luminosity function with the limit previously derived for the *Kepler* field (Kennedy & Wyatt 2012). Stars in the *Kepler* field are much fainter than nearby stars, and the number and distribution of detected excesses is consistent with that expected from chance alignments with background galaxies. The distribution

---

[6] *WISE* did not survive an entire year, so the whole sky was not observed twice (Wright et al. 2010). Here, we have not used the so-called 3-Band Cryo data release as any variability found would remain in question due to the change in cooling after the end of the full cryogenic mission.

Figure 5. Luminosity function at 12 μm for Sun-like *Hipparcos* stars (black line with dots). The black dashed line shows the *WISE* detection limit of 0.15. Also shown are the limits from the Kepler field (grey line; Kennedy & Wyatt 2012). The *Hipparcos* line most likely lies above the Kepler field line due to small number variation.

derived here lies slightly above the limit from the *Kepler* field at the bright end, which most likely arises due to small number variation, though could also be suggesting that the brightest excesses in the *Kepler* field are in fact real but not very robust against background galaxy confusion.

Given the clear bias towards young stars among our excess candidates, the dark lines with added dots in both panels of Fig. 6 show our luminosity function split by age (the grey lines are models, described below). 'Young' stars are those younger than 120 Myr and 'old' stars are those older than 1 Gyr (our warm dust sample has no stars between 120 Myr and 1 Gyr, see also Section 5.3). This split requires us to use the age distribution shown in Fig. 2, for which the number of young stars is 607, and the number of old stars is 19 114. The distributions in Fig. 6 therefore divide the detections by these total number estimates. Stars with unknown ages are added to each group to illustrate the possible uncertainty in each distribution. The
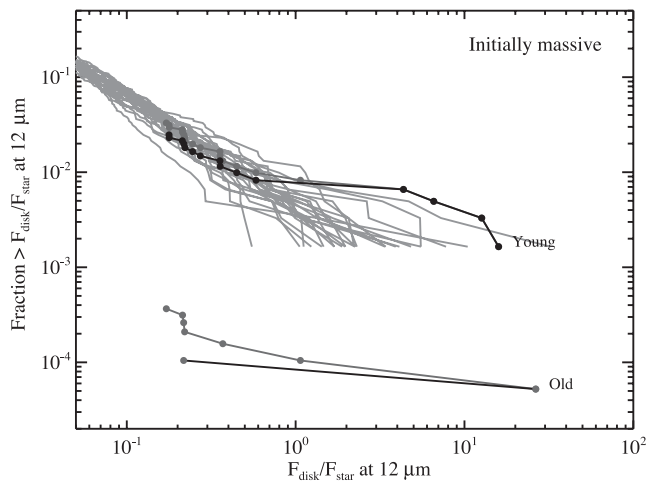
main point here is that old warm dust systems are extremely rare, while young ones are not.

5 IN SITU EVOLUTION

One powerful advantage of knowing the distribution of warm excesses is that it contains information about how discs evolve. For example, a population of discs whose brightness decays as 1/time, that is observed at random times would be distributed with a slope of −1 in Fig. 5. A disc spends 10 times longer in each successive decade of luminosity than it did in the previous one, so every bright disc that is discovered is the tip of an iceberg of fainter discs that are decaying evermore slowly.

Our basic assumption in now making a model to compare to our derived luminosity function is that warm dust arises from some in situ process, for example a collision or collisions between parent bodies that normally reside where the dust is observed. In the alternative comet delivery scenario, where objects are injected from elsewhere (i.e. larger radial distances), no well-informed population evolution model can currently be made because the behaviour depends on the detailed dynamics of each individual system, how those dynamics change over time and how systems with the appropriate dynamics are distributed. Of course, this difficulty does not mean that comet delivery is a less viable scenario; we discuss it further in Section 6.2.

5.1 Model description

Our goal is therefore to use an in situ evolution model and apply it to the observed 12 μm luminosity function, testing different scenarios and making predictions for surveys that probe fainter dust. The model described below has been outlined in previous works (Wyatt et al. 2007a,b; Wyatt 2008). The basic premise is that a size distribution of objects is created in catastrophic collisions between a reservoir of the largest objects. The resulting 'collisional cascade' size distribution remains roughly constant in shape (Dohnanyi 1969), so the dust level (i.e. the number of smallest objects) is proportional to the number of the largest objects. To connect the mass with the observed dust level requires a relation between the total mass M_{tot}
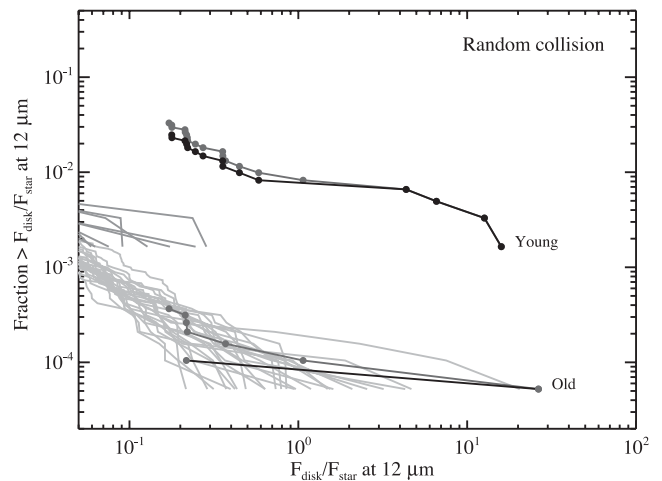
Figure 6. Monte Carlo evolution simulations. Lines with dots show the observed luminosity function, and the grey lines show 25 realizations of the model in the young (darker grey, 0–120 Myr) and old (lighter grey, 1–13 Gyr) age bins. Left-hand panel: initially massive scenario, showing that young discs are well explained but that old discs are not expected at a level visible in this plot. Right-hand panel: random collision scenario, showing that if old discs are explained, young stars do not have a sufficient number of bright discs to match those observed (i.e. the handful of dark grey lines near $F_{disc}/F_\star \sim 10^{-2}$ are well below the observed line for young stars).

and the total surface area σ_{tot}, which depends on the maximum and minimum object sizes D_{min} and D_c, and the slope of the size distribution q, where the number of objects between D and $D + dD$ is $n(D) = K D^{2-3q}$ (Wyatt et al. 2007b)

$$M_{tot} = 2.5 \times 10^{-9} \frac{3q-5}{6-3q} \rho \sigma_{tot} D_{min} \left(10^9 D_c / D_{min}\right)^{6-3q}, \qquad (1)$$

where M_{tot} is in units of $M_\oplus$, ρ is the planetesimal density in kg m^{-3}, σ_{tot} is in au^2, D_{min} is in μm and D_c in km. With $q = 11/6$, the total mass is dominated by the largest objects and the total surface area by the smallest grains. To now connect the surface area with the observed dust level, we assume that the dust emits as a pure blackbody, so

$$F_{\nu,disc} = 2.4 \times 10^{-11} B_\nu(\lambda, T_{disc}) \sigma_{tot} d^{-2}, \qquad (2)$$

where B_ν is the Planck function in Jy sr^{-1} and d is the distance to the star in parsec. We approximate the stellar emission as

$$F_{\nu,\star} = 1.8 B_\nu(\lambda, T_\star) L_\star T_\star^{-4} d^{-2}, \qquad (3)$$

where the stellar luminosity $L_\star$ is in units of $L_\odot$ and the effective temperature $T_\star$ is in K. We define ξ_ν as the disc-to-star flux ratio at some wavelength

$$\xi_\nu \equiv \frac{F_{\nu,disc}}{F_{\nu,\star}} = 1.3 \times 10^{-11} \frac{B_\nu(\lambda, T_{disc})}{B_\nu(\lambda, T_\star)} \sigma_{tot} T_\star^4 L_\star^{-1}. \qquad (4)$$

With equations (1) and (4) and some assumed planetesimal properties we are therefore able to link an excess observed at some wavelength and temperature with the total mass in the disc.

Because the size distribution is such that most of the total mass M_{tot} is contained in the largest objects, the dust level decays at a rate proportional to the large object collision rate, which has a characteristic time-scale t_{coll} (in Myr)

$$t_{coll} = 1.4 \times 10^{-9} r^{13/3} (dr/r) D_c \, Q_D^{\star \, 5/6} \, e^{-5/3} M_\star^{-4/3} M_{tot}^{-1}, \qquad (5)$$

where dr is the width of the belt at r (both in au), $Q_D^\star$ is the object strength (J kg^{-1}) and e is the mean planetesimal eccentricity, and $M_\star$ is the stellar mass. The disc radius can be expressed in terms of temperature with

$$T_{disc} = 278.3 L_\star^{1/4} r^{-1/2}. \qquad (6)$$

The mass-loss rate is $dM_{tot}/dt \propto M_{tot}^2$ and the mass decays as (Dominik & Decin 2003)

$$M_{tot} = M_{tot,0} / (1 + t/t_{coll,0}), \qquad (7)$$

where t is the time since the evolution started and $M_{tot,0}$ was the mass available for collisions at that time (with a consequent collision time-scale $t_{coll,0}$). This time may be the age of the host star t_{age}, but may be smaller, for example if the belt was generated from a collision event that was the result of a dynamical instability well after the star and planets were formed. An equivalent equation also applies to the disc-to-star flux ratio

$$\xi_\nu = \xi_{\nu,0} / (1 + t/t_{coll,0}). \qquad (8)$$

Though numerical models find that the evolution can be slower than 1/time (e.g. Löhne et al. 2008; Gáspár, Rieke & Balog 2013), these results are based on discs at large semimajor axes where the largest objects are not in collisional equilibrium. For example, though Löhne et al. (2008) state that their discs decay as $t^{-0.3 \text{ to } -0.4}$, they also note that both the disc and dust masses tend to 1/time decay at times that are sufficiently late such that the largest objects have reached collisional equilibrium. Gáspár et al. (2013) find a much slower $t^{-0.08}$ mass decay for their reference model. However,

the slow decay appears to be because the largest (1000 km) objects in their size distribution have not started to collide, even at the latest times, and hence the total mass (which is dominated by these objects) is only decaying due to the destruction of smaller objects (the lack of 1000 km object evolution for their reference model can be seen in fig. 1 of Gáspár et al. 2012). Because the warm discs we consider here are very close to their central stars (i.e. a few au) and the collision rate scales very strongly with radius (equation 5), collisional equilibrium is reached in only a few Myr (which we also confirm a posteriori). Therefore, we consider that while our analytic model is necessarily simplified, a 1/time evolution is justifiably realistic.

5.2 Model implementation and interpretation

To implement the model, we simply assume some initial disc brightness ξ_ν and that the collision time-scale has the same form as equation (5)

$$t_{coll,0} = C / \xi_{\nu,0} \qquad (9)$$

so C has units of time in Myr and is shorter for discs that are initially more massive, being the collision time for a disc of unity $\xi_{\nu,0}$ (and some equivalent $M_{tot,0}$ that can be calculated using equations 1 and 4). For our model, C is the only variable parameter.

To interpret C in terms of physical parameters we combine equations (1), (4) and (5), and rewrite the answer in terms of C, giving

$$C = 7.4 \times 10^{-12} \frac{r^{13/3}}{\rho} \frac{dr}{r} \left(\frac{1}{10^9} \frac{D_c}{D_{min}}\right)^{3q-5}$$

$$\times \frac{T_\star^4}{M_\star^{4/3} L_\star} \frac{B_\nu(\lambda, T_{disc})}{B_\nu(\lambda, T_\star)} \frac{6-3q}{3q-5} Q_D^{\star \, 5/6} e^{-5/3}. \qquad (10)$$

Because the collision time-scale depends on the disc mass (or equivalently brightness), C does not depend on the initial disc mass (see Wyatt et al. 2007a), but on a number of other parameters, most of which we can estimate values for. We assume a Sun-like host star with $L_\star = 1 \, L_\odot$, $T_\star = 5800$ K and $M_\star = 1 \, M_\odot$. We assume that the disc lies at 1 au and hence $T_{disc} = 278.3$ K, and that $dr = 1$. We assume a size distribution slope of $q = 11/6$. Finally, we include the wavelength of observation, $\lambda = 12$. With these assumptions equation (10) reduces to

$$C = 3.1 \times 10^{-7} \sqrt{\frac{D_c}{D_{min}}} Q_D^{\star \, 5/6} e^{-5/3}. \qquad (11)$$

The remaining parameters are therefore the maximum and minimum planetesimal sizes, their strengths, and their eccentricities. We may further assume that the minimum grain size is $D_{min} = 1$ μm, the approximate size at which grains are blown out by radiation pressure from solar-type stars. The coefficient for this equation does not change strongly with spectral type, and for example is 5×10^{-7} for an early F-type star, assuming that the dust remains at the same temperature (i.e. has a larger radius of about 2.5 au) and that the minimum grain size has increased to 4 μm due to the increased luminosity.

5.3 Excess evolution

In order to test the expectations for disc evolution, we use the evolution model described above to construct two simple Monte Carlo models of 12 μm evolution. In the first 'initially massive' scenario, all stars have relatively massive and bright warm discs at early times

(see Section 6.1 for further discussion of how this scenario could be interpreted). In this picture, the time since the onset of decay is simply the stellar age. All stars have discs regardless of age, but these become progressively fainter for populations of older stars. In the second 'random collision' scenario, stars have a single dust creation event at some random time. Though we have a range of spectral types, we set the epoch of this event to be a random time between 0 and 13 Gyr because it is unlikely to be related to stellar evolution (the time distribution of these events is however revisited in Section 6.1). Our age distribution means that many stars will be observed before such a collision happens (see Section 4.5), though this detail does not affect the model because it is degenerate in the sense that multiple (instead of single) collisions could be invoked and offset by a shorter collision time to yield the same results. Only those stars that happen to have a collision at a young age and are observed at a young age will have a detectable excess.

We assume that stars have the age distribution shown in Fig. 2. The initial distribution of flux ratios for both models is assumed to be log normal with zero mean and unity dispersion in $\log(F_{\rm disc}/F_\star)$, so covers the bright end of the luminosity function. We found that the choice of initial distribution does not strongly influence the results, and for example a power-law distribution weighted towards fainter levels but with some bright discs yields very similar results.

We generate discs according to each scenario using two age bins; those that are 'young' (<120 Myr) and those that are 'old' (>1 Gyr), using the same numbers of stars noted in Section 4.5 (607 young stars and 19 114 old stars). We restrict the old stars to be older than 1 Gyr because BD+20 307 is ~ 1 Gyr old, whereas placing the cut at >120 Myr results in disc detections in the old group that are not much older than 120 Myr, so not as old as the stars we wish to compare the model with. While there are other possible choices of bin locations, the point is that warm excesses around young stars are common, and those around old stars are not, which allows us to distinguish between the models outlined above. In each bin we generate 25 model realizations to illustrate the scatter due to small numbers. The only model parameter is C, which sets how rapidly discs decay, and is varied by hand so that the synthetic distributions have approximately the same level as those observed.

The results from the two models are shown in Fig. 6. The left-hand panel shows the initially massive warm belt scenario, while the right-hand panel shows the random collision scenario. Looking first at the initially massive panel, while reasonable agreement is obtained for young stars, no old stars are seen to have large excesses as the dust has decayed significantly by Gyr ages (these discs have $F_{\rm disc}/F_\star \sim 10^{-3}$, see 1–2 Gyr dotted line for initially massive warm discs in Fig. 9). This result echoes the conclusions of Wyatt et al. (2007a), who found that bright debris discs around old stars cannot arise from the in situ evolution considered in this scenario. The observed young star distribution is usually flatter than most of the models, which might be explained by extra physical processes not included in our model. We note a few of these in Section 6.1.

Turning now to the right-hand panel of Fig. 6, the random collision scenario reasonably reproduces the luminosity function of warm dust around old stars, but fails to match those seen around young stars. The chance that at least some of these are young, and the possibility that HD 150697 is in fact young, means that a somewhat larger value of C (slower evolution) could be used to find better agreement with BD+20 307 (i.e. shift the model lines upward, thereby making dust from random collisions more common). This slower evolution would however predict about 10 times more systems with $F_{\rm disc}/F_\star \gtrsim 0.15$ that are not observed. While a few young systems are seen to have excesses due to random collisions

(about 1 per cent at $F_{\rm disc}/F_\star \sim 0.1$), these are too infrequent to match the relatively high occurrence rate that is observed. The conclusion is perhaps obvious; if collisions occur randomly over time it is unlikely that a young star will have a collision that is observed soon afterwards. The rapid collisional evolution means that even if they are, the dust levels are unlikely to be extreme.

The only significant model parameter is C, which is set to 1 Myr for both scenarios and provides reasonable agreement with the observed luminosity function in each case. This parameter need not be the same, as the scenarios could for example have very different sized parent bodies or random velocities. As outlined above in Section 5.2, for various assumptions C can be interpreted in terms of physical system parameters. Assuming $D_{\rm min}=1$, equation (11) implies that $D_{\rm c}^{1/2}\left(Q_{\rm D}^\star\right)^{5/6}e^{-5/3}=3.2\times10^6$. This value can be compared to previous results for this combination, for example Wyatt et al. (2007b) found 7.4×10^4 for the evolution of Kuiper belt analogues around A stars, and Kains, Wyatt & Greaves (2011) found 1.4×10^6 for Kuiper belt analogues around Sun-like stars (i.e. both were for discs at much larger radii than those considered here). The latter authors discuss possible reasons for the large difference, which could arise due to real differences between planetesimal populations around A-type and Sun-like stars, or due to differences in the observables such as the 24–70 µm colour temperature, which could change due to different grain blowout sizes for example. The point here is that the resulting C is sensible compared to previous results. If it were significantly different the plausibility of the in situ scenario would be questionable.

To create an in situ picture that explains significant levels of warm dust around both young and old stars clearly requires some combination of our two scenarios. We therefore make a simple combined model where systems start with the same initial distribution of warm excesses and also have a single random collision at some point during their lifetimes. This model has the same value of $C=1$ Myr as before, and is shown in Fig. 7. Given that each respective scenario dominates the young and old populations with little effect on the other, the fact that the model is in reasonable agreement with the observed luminosity function is unsurprising. One or two random collisions may be present in the young population of discs, and all old stars have initially massive belts that are now very faint. This model could be tuned a little more by specifying the fraction of systems that are initially massive and/or those that undergo
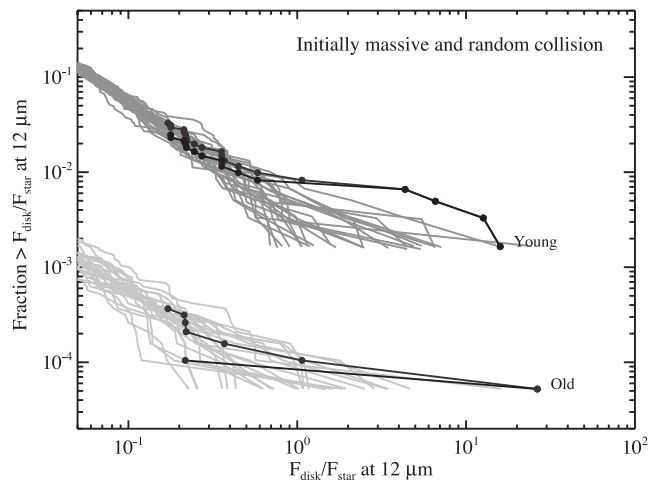
Figure 7. Same as Fig. 6, but for a model that combines both initially massive warm belts and a single collision at a random time during the main-sequence lifetime.

collisions. However, the agreement shown in Fig. 7 is good enough to illustrate that such a picture matches the observed distribution well. Therefore, we conclude that the Monte Carlo evolution model could be a realistic (though not uniquely so) description of the origins of warm dust. This model is of course highly simplified and largely empirical, and we discuss some issues further in Section 6.1.

Though we have shown that it is sensible, the assumption of in situ decay made by the above model may not be correct, with material being delivered to the terrestrial regions from elsewhere, in which case the apparently sensible value of the parameter C is coincidental. In a comet delivery scenario, it is likely that the luminosity function is not the same as expected for $1/t$ evolution (though it could be). One test of our model is therefore to extrapolate to fainter levels, where detections are possible with much more sensitive observations of relatively few stars.

5.4 Extrapolation to faint exo-Zodi levels

The level of dust around a 'typical' Sun-like star is a key unknown and crucial information needed for the future goal of imaging Earth-like planets around other stars (e.g. Beichman et al. 2006; Absil et al. 2010; Roberge et al. 2012). There are several avenues for finding the frequency of warm dust at relatively low levels; either to directly detect it around an unbiased sample of stars (e.g. Millan-Gabet et al. 2011) or to make predictions based on the expected evolution of brighter dust. The former approach is clearly preferred as it yields a direct measure, but finding such faint dust is technically difficult and is the focus of dedicated mid-IR instruments such as the Bracewell Infrared Nulling Camera at the Multiple Mirror Telescope (MMT; Liu et al. 2009), the Keck Interferometer Nuller (KIN; Colavita et al. 2009) and the Large Binocular Telescope Interferometer (LBTI; Hinz 2009).[7] These instruments are more sensitive to warm dust than photometric methods because their sensitivity is set by their ability to null the starlight and detect the astrophysical flux that 'leaks' through the fringes (e.g. Millan-Gabet et al. 2011). The typical scale on which these mid-IR instruments are sensitive is 10–100 mas so are well suited to the terrestrial regions around the nearest stars. The latter approach of extrapolating results from less sensitive photometric surveys based on evolution models (i.e. the approach here) is easier in the sense that data for bright warm dust systems are readily available, but is of course more uncertain due to the unknown origin and evolution of these systems. A future goal is to fold the results from interferometry back into the modelling process.

Fig. 8 shows the 12 μm luminosity function and one realization of the combined initially massive and random collision model for 0–13 Gyr old stars over a wider disc–star flux ratio range than Fig. 6, using our adopted age distribution. The model underpredicts the number of brightest excesses, as this is the typical outcome (as shown in Fig. 7), but varies considerably due to the small number of such discs. Below $F_{\rm disc}/F_\star \sim 0.1$ all realizations, and hence the predictions for fainter discs, are very similar.

The right-hand side of the figure is covered by photometric surveys like the one presented here, whereas fainter discs (left-hand side) can only be detected with more sophisticated methods, such as those employed by the KIN and LBTI. We have taken the approximate Solar system 12 μm dust level as $F_{\rm disc}/F_\star = 5 \times 10^{-5}$,
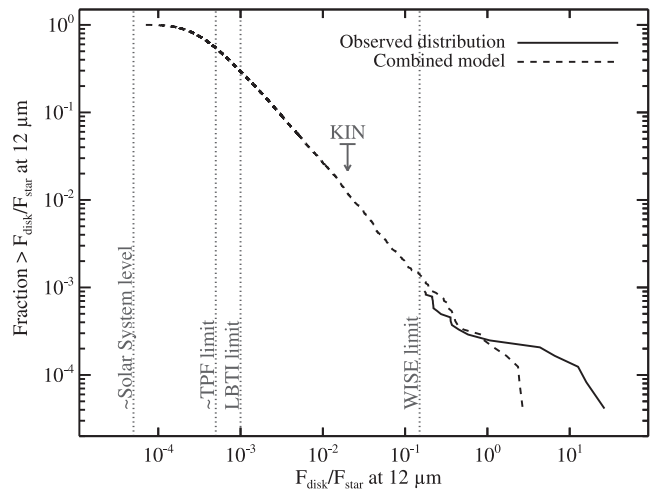
Figure 8. Observed luminosity function (solid line) and a simple prediction for faint exo-Zodi for stars between 0 and 13 Gyr with a single realization of the combined initially massive and random collision model shown in Fig. 7 (dashed line). The grey dotted lines show the limits for LBTI and *WISE* sensitivity, as well as approximate levels for the Solar system Zodiacal cloud and for which *TPF*-like missions will be compromised by exo-Zodi. The upper limit from the 23 star KIN survey is also shown (see the text).

and the LBTI sensitivity as 20 times this level (Hinz 2009). The predicted limit for exo-Earth detection by a *Terrestrial Planet Finder* (*TPF*)-like mission is also shown (at 10 times the Solar system level).[8]

The limit set by the KIN survey (Millan-Gabet et al. 2011), which resulted in no significant detections, is shown, but merits further discussion. Their sample was classified into 'high' and 'low' dust systems, meaning those with or without detections of cool Kuiper belt analogues. Of the 25 systems observed, two were high dust systems (η Corvi and γ Ophiuchi) and warm dust was confidently detected around the former. η Crv is already well known to have distinct warm and cool dust belts (Wyatt et al. 2005; Smith, Wyatt & Dent 2008), while only cool dust has been detected around γ Oph (Sadakane & Nishida 1986; Su et al. 2008). We use the other 23 low dust stars in calculating the KIN limit, with the caveat that if warm dust levels are positively (or negatively) correlated with cool dust levels, the limit will be slightly too low (or too high). Given that only ~20 per cent of stars are seen to have cool dust (i.e. many low dust systems could still have relatively high dust levels that could not be detected) this bias will not be very strong.

For stars drawn randomly from our assumed age distribution, the predicted disc fraction is about 50 per cent at the LBTI sensitivity. Future work may however show that our assumption of $1/t$ evolution is not exactly correct; the fraction decreases to 10 per cent, if the decay is instead $t^{-1.5}$ so the prediction is not extremely sensitive to the decay rate. A very slow decay, such as that seen in the reference model of Gáspár et al. (2013) would appear to be ruled out by the KIN upper limit as it would predict many bright warm discs (such slow evolution is not expected for warm discs anyway, see the end of Section 5.1). It is in any case clear that an unbiased LBTI survey of just a few tens of stars would result in a strong test of our prediction, and has the potential for detection of a dozen or so discs if the

---

[7] Several near-IR interferometers have also been used to search for exo-Zodi, though these are more sensitive to dust temperatures of ~1000 K (e.g. Absil et al. 2006, 2013; Defrère et al. 2011; Mennesson et al. 2011).

[8] In the sense that integration times become too long for a worthwhile mission for some reasonable assumptions, not that detection is impossible (Roberge et al. 2012).
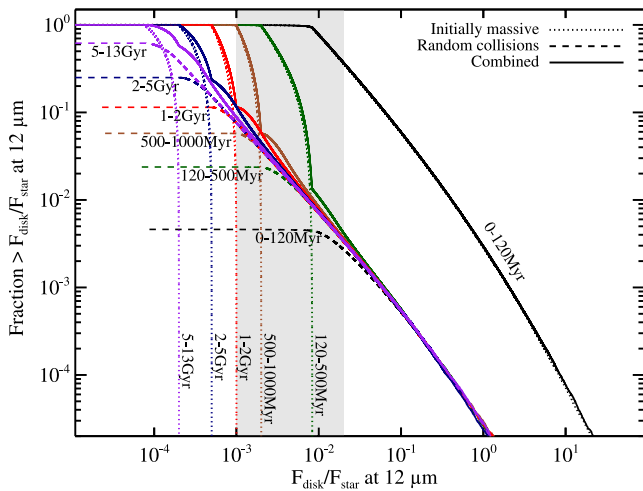
Figure 9. Similar to Fig. 8, but showing the contribution of initially massive discs (dotted lines) and random collisions (dashed lines) and the combined model (solid lines). Stars are shown in different age bins given by boundaries of: 0, 120, 500, 1000, 2000, 5000 and 13 000 Myr. The region where the predicted LBTI sensitivity improves over the KIN is marked with a grey band. Older systems have lower dust levels from the initially massive contribution, and the underlying level from random collisions dominates.

evolution predicted by our model is correct. Such a result would be a great success for the instrument, but less promising for the study of exo-Earths; another prediction of our model is that roughly only a few tens of per cent of stars are amenable to exo-Earth detection if our combined model is correct.

We have already shown that the different scenarios depend strongly on the age of the stellar population that is observed. This effect is shown explicitly in Fig. 9, which shows the individual and combined distributions in a series of age bins. Here, we have increased the number of stars in each age bin to 10^7 so that the curves are smooth. For both dust creation scenarios, the level of the faintest systems decreases with time as the stars become older. However, because random collisions can happen at any time, the luminosity function for these events is otherwise independent of time. The initially massive population dominates the distribution for stars younger than about 100 Myr, but becomes much less important as time goes on. For stars that are older than ~500 Myr the brightest excesses are already dominated by random collisions if our model is correct.

The solid lines show the combined model, which generally follow the fraction set by the model that dominates at a given disc-to-star flux ratio. At flux ratios where both components contribute to a similar fraction of systems (i.e. just above the maximum ratio for initially massive belts), the fraction is somewhat greater than expected just for random collisions. This increase arises because for these systems the emission from random collisions is augmented by dust that was initially bright (but is now much fainter).

This comparison of scenarios shows that for the oldest main-sequence stars the predicted frequency of dust systems is lower than shown in Fig. 8. The faintest dust may still come from those that were initially massive, but the bulk of the population are remnants of random collisions. That is, though the random collisions are very rare and are only bright for a short period of time, their decay through lower levels means that they may in fact dominate the bulk of the warm dust luminosity function for main-sequence stars.

6 DISCUSSION

6.1 In situ evolution

We have described a simple model of in situ evolution that reproduces the observed distribution of 12 μm excesses reasonably well. This model has two components, an initially massive component and a random collision component, both of which are needed to simultaneously explain relatively frequent warm dust around young stars and extremely rare warm dust around ~Gyr old stars (Fig. 7). The predicted luminosity function changes strongly with age due to the different contribution from each component (Fig. 9). However, the ~Gyr old bright warm dust systems imply an underlying population of fainter warm dust that is present, regardless of age. Therefore, if our model is correct, the fraction of stars with warm dust levels sufficient to hinder exo-Earth detection may be a few tens of per cent, even if only old stars are targeted.

By using the term 'initially massive' for the disc component that is bright at early times, we have implied that it is a pumped-up version of our own Asteroid belt. While such an interpretation may be correct, an alternative possibility is that large amounts of warm dust are generated in the first ~100 Myr as a by-product of terrestrial planet formation (Kenyon & Bromley 2004; Lisse et al. 2008, 2009; Jackson & Wyatt 2012). Such a scenario evolves similar to an initially massive Asteroid belt analogue, but is different in a few specific ways; the dust levels may initially increase as large planetary embryos that stir the planetesimals to destructive collision velocities form, dust may be visible for longer as mass is released from embryos in planet forming impacts, and planetesimals and dust may also be depleted by dynamical interaction with the embryos. These differences mean that the emission from terrestrial planet formation may not simply decay as 1/time, providing a potential way to distinguish it from initially massive Asteroid belt analogues (e.g. Currie et al. 2008).

One limitation of our model is that processes beyond the basic collisional evolution will modify the model luminosity functions. As noted above, dynamical depletion may follow catastrophic collision events, perhaps with an initially optically thick phase (Jackson & Wyatt 2012). Significant variability and non-linear decay could also arise at early stages due to changes in dust mineralogy. For example, the silicate peak near 12 μm could decrease in strength after a collision event as the smallest grains are removed by radiation pressure. The overall dust level may also vary following the initial creation event as the system settles into dynamical and collisional equilibrium. Such processes might be responsible for the observed luminosity function being somewhat flatter than the models (Figs 6–8).

A more basic limitation is our implementation of random collisions. With only a few warm dust sources around ~Gyr old stars there is little leverage to constrain models, so this part of our model is necessarily simple, and not, for example, linked to the mass remaining from initially massive belts. The largest simplification is that the uniform probability of a collision over 0–13 Gyr assumed here is unlikely to be the case. Wyatt et al. (2007a) showed that if these collisions are between the largest objects in a continuous size distribution (i.e. just the largest objects in an Asteroid belt analogue), then the probability of detecting a collision drops as $1/time^2$. An alternative possibility is that the collisions are between individual large objects (e.g. planets or planetary embryos) that simply did not collide earlier, or were perhaps subject to some late instability. These objects may have originally been part of a continuous size distribution, but were 'stranded' when only a

few remained and their chances of destruction became much lower (see Kennedy & Wyatt 2011). However, in these cases collisions are more likely to occur at earlier times, though perhaps with a weaker dependence compared to the large asteroid scenario just described.

That the 'old' stars hosting warm dust, BD+20 307 and possibly HD 150697 are between 1 and 4 Gyr old can be used to illustrate that there is a rough constraint on the time dependence of random collisions. This constraint is uncertain because in our sample there are five sources of unknown age, and the ages of some others are poorly constrained. However, a $1/\text{time}^2$ dependence is not favoured because the existence of warm dust around the $\sim$Gyr old stars implies that a significant number should exist around stars with ages from $\sim$100–1000 Myr, which are not observed. The argument is similar for $1/\text{time}$, but given the uncertainties is harder to rule out. Similarly, for the random collision model with uniform time dependence a few detections are expected in the 4–13 Gyr age bin and these are not observed either. Therefore, if the random collision scenario is correct the time dependence of collisions must decrease with time fairly weakly, if at all.

6.2 Comet delivery

While we so far have discussed our observational results in the context of an in situ model of evolution, the observed dust may originate elsewhere. Specifically, material may be delivered from more distant regions after interacting with planets, thus replenishing the mass that resides in the warm belt (e.g. Bonsor & Wyatt 2012; Bonsor et al. 2012). With this kind of evolution, the observed emission need not decay as $1/t$, and the luminosity function need not have the slope of -1 seen in Fig. 8.

Such a scenario may be acting to replenish the Zodiacal cloud in the Solar system. The Zodiacal dust was first suggested to arise from particles dragged radially inwards from the Asteroid belt by Poynting–Robertson drag (Kresak 1980). More recently, however, Nesvorný et al. (2010) have shown that most of the Zodiacal cloud as seen by *IRAS* can be explained by a sufficient level of spontaneous disruptions of Jupiter-family comets (though the existence of dust bands means that Asteroid families still contribute some dust; Dermott et al. 1984). Because Jupiter-family comets are themselves thought to originate in the Edgeworth–Kuiper belt (Levison & Duncan 1997), the location in which the dust is observed (i.e. near Earth) is only linked to the source region by comet dynamics, which are dominated by the Solar system's four giant planets.

In this kind of scenario, the amount of warm dust is plausibly linked to the number of comets in the source region; a change in the number of source objects should be directly reflected in the number scattered inwards, and therefore be reflected in the observed dust level. Therefore, if the source region is in collisional equilibrium at all sizes (i.e. $M_{\text{tot}} \propto 1/t$), then the observed dust level should decay as roughly $1/t$, with some additional contribution from dynamical depletion (that may be strongest at early times). While the possibility of $1/t$ decay might appear consistent with the model of Section 5, a very different value for the decay time-scale C is expected because collisional evolution is much slower at larger radial distances (i.e. at least Gyr instead of Myr; Trilling et al. 2008). Therefore, a naive picture of warm dust occurring in all systems exclusively due to a uniformly initially bright level of steady delivery throughout the main sequence does not work because the brightest systems are not predicted to be rare; their Gyr decay times mean that they should in fact be ubiquitous. The

problem with this picture is that comet delivery will not always be initially bright; the level is set by the dynamics of individual systems. It may be that near constant comet delivery is the dominant warm dust origin and the luminosity function is set entirely by the distribution of systems with the appropriate dynamics (Bonsor & Wyatt 2012).

Though we have argued for the slow decay of reservoirs from which comets are delivered, it is also possible that a comet delivery scenario could mimic our initially bright asteroid belt analogues or terrestrial planet formation due to the planetary system dynamics in the first $\sim$100 Myr. A newly formed planetary system will have small bodies scattered throughout, and in addition to those in young Asteroid and Kuiper belt analogues, many will also be on unstable orbits. These unstable objects could contribute to warm dust levels as they are cleared over the first 100 Myr or so, thus appearing to decay in the same way as initially massive belts.

Clearly, more work is needed to explore the likelihood of in situ and cometary origins for warm dust. For example, it could be that warm dust originates in some cases from an impact on an object orbiting at $\sim$1 au by an interloping comet (e.g. Lisse et al. 2012), in which case the material is terrestrial in origin and evolves as such (i.e. in situ), but whose probability of occurrence is more closely related to the comet delivery rate.

6.3 Solar system comparison

A basic prediction of our model is that the level of Zodiacal dust seen in the Solar system is roughly a factor of 10 fainter than is typical (Fig. 8). Given the uncertainties discussed above this predicted rarity is not an issue for our model, but worth some consideration.

If the bulk of our Zodiacal light comes from the Asteroid belt, the lower than predicted dust level could arise in several ways. The initial distribution may simply have more faint belts than we assumed, reflecting the range of outcomes dictated by planetesimal growth in the protoplanetary disc or other processes such as planet migration. For example, in the Solar system the Asteroid belt is thought to have been severely dynamically depleted when Jupiter formed (Petit, Morbidelli & Chambers 2001), and a more general inner Solar system depletion may have occurred if Jupiter was at some point closer to the Sun that it is now (Walsh et al. 2011). This difference could be accounted for by weighting the initial brightness distribution towards lower levels, with a slower disc decay rate to keep the same number of observed warm discs.

If the bulk of our Zodiacal light comes from comet delivery, it may again be that the true initial distribution is different to that assumed here, or that the evolution is not continuous as assumed in our model. For example, it could be that the Solar system's Zodiacal cloud evolution was interrupted by a late dynamical instability that ejected of most of the primordial Kuiper belt (Tsiganis et al. 2005). Removal of most of the source region mass would cause the warm dust level to drop in a way not accounted for by our model. While it is currently unknown if the Kuiper belt has a relatively low mass (e.g. Greaves & Wyatt 2010), the relative faintness of the Zodiacal cloud in the comet delivery picture could be explained if such depletion events are relatively uncommon around stars in general.

Naturally, many of the possible extensions to our model could involve the effect of planets on the parent planetesimals, whether they be asteroids or comets. Therefore, in addition to looking for correlations between warm and cold dust as a signature of scattering by planets (Absil et al. 2013), an important goal is to look for correlations between warm dust and planets. While a tentative positive correlation has been seen between low-mass planets and

cool Kuiper belt analogues (Wyatt et al. 2012), no trends have yet been seen for warm dust (e.g. Morales et al. 2012).

7 SUMMARY AND CONCLUSIONS

We have presented an analysis of the bright end of the 12 μm warm dust luminosity function as seen by *WISE* around nearby Sun-like stars. We report the possible detection of six new warm dust candidates, HD 19257, HD 23586, HD 94893, HD 154593, HD 165439 and HD 194931.

There is a clear preference for excess emission around young stars, with at least 14/22 systems younger than 120 Myr, despite the ~10 Gyr stellar lifetime. However, one of the dustiest systems is ~1 Gyr old, and another may have a similar age, suggesting that while youth is an important factor for setting the brightness of warm dust, it is not the sole factor.

Using a simple in situ evolution model to interpret the observed luminosity function, we show that neither a picture where all systems have initially massive discs, nor one where all excesses are due to randomly timed collisions, can explain the fact that warm dust is observed around both young and old stars. A simple combination of these two in situ scenarios reproduces the observed luminosity function. However, we cannot rule out that warm dust is in fact dominated by comet delivery. In this scenario, comets are scattered from a more distant reservoir, and reliable luminosity function predictions cannot be made because they depend on the distribution of systems with the appropriate dynamics.

We have made simple predictions for the number of exo-Zodi that might be detected by an unbiased LBTI survey. For the expected sensitivity we anticipate a handful of detections and a strong test of our evolution model. Such tests are a crucial step towards understanding the origins and evolution of exo-Zodi, and ultimately the imaging of Earth-like planets.

REFERENCES

Absil O. et al., 2006, A&A, 452, 237
Absil O., Eiroa C., Augereau J., Beichman C. A., Danchi W. C., Defrère D., Fridlund M., Roberge A., 2010, in Coudé Du Foresto V., Gelino D. M., Ribas I., eds, ASP Conf. Ser. Vol. 430, Pathways Towards Habitable Planets. Astron. Soc. Pac., San Francisco, p. 293
Absil O. et al., 2013, A&A, submitted
Andrews S. M., Czekala I., Wilner D. J., Espaillat C., Dullemond C. P., Hughes A. M., 2010, ApJ, 710, 462
Aumann H. H., Probst R. G., 1991, ApJ, 368, 264
Beichman C. A. et al., 2005, ApJ, 626, 1061
Beichman C. A. et al., 2006, ApJ, 652, 1674
Beichman C. A. et al., 2011, ApJ, 743, 85
Bessell M. S., 2005, ARA&A, 43, 293
Bonsor A., Wyatt M. C., 2012, MNRAS, 420, 2990
Bonsor A., Augereau J.-C., Thébault P., 2012, A&A, 548, A104
Booth M. et al., 2013, MNRAS, 428, 1263
Brott I., Hauschildt P. H., 2005, in Turon C., O'Flaherty K. S., Perryman M. A. C., eds, ESA Special Publication, Vol. 576, The Three-Dimensional Universe with Gaia. ESA, Noordwijk, p. 565
Carmona A., van den Ancker M. E., Audard M., Henning T., Setiawan J., Rodmann J., 2010, A&A, 517, A67
Carpenter J. M., Mamajek E. E., Hillenbrand L. A., Meyer M. R., 2009, ApJ, 705, 1646
Chen C. H., Jura M., Gordon K. D., Blaylock M., 2005, ApJ, 623, 493
Chen C. H., Mamajek E. E., Bitner M. A., Pecaut M., Su K. Y. L., Weinberger A. J., 2011, ApJ, 738, 122
Chen C. H., Pecaut M., Mamajek E. E., Su K. Y. L., Bitner M., 2012, ApJ, 756, 133
Clarke C. J., Gendrin A., Sotomayor M., 2001, MNRAS, 328, 485
Clarke A. J., Oudmaijer R. D., Lumsden S. L., 2005, MNRAS, 363, 1111
Colavita M. M. et al., 2009, PASP, 121, 1120
Currie T., Kenyon S. J., Balog Z., Rieke G., Bragg A., Bromley B., 2008, ApJ, 672, 558
de Zeeuw P. T., Hoogerwerf R., de Bruijne J. H. J., Brown A. G. A., Blaauw A., 1999, AJ, 117, 354
Defrère D. et al., 2011, A&A, 534, A5
Dermott S. F., Nicholson P. D., Burns J. A., Houck J. R., 1984, Nat, 312, 505
Dohnanyi J. S., 1969, J. Geophys. Res., 74, 2531
Dominik C., Decin G., 2003, ApJ, 598, 626
Fajardo-Acosta S. B., Beichman C. A., Cutri R. M., 2000, ApJ, 538, L155
Fazio G. G. et al., 2004, ApJS, 154, 10
Fujiwara H. et al., 2010, ApJ, 714, L152
Fujiwara H., Onaka T., Yamashita T., Ishihara D., Kataza H., Fukagawa M., Takeda Y., Murakami H., 2012a, ApJ, 749, L29
Fujiwara H., Onaka T., Takita S., Yamashita T., Fukagawa M., Ishihara D., Kataza H., Murakami H., 2012b, ApJ, 759, L18
Fujiwara H. et al., 2013, A&A, 550, A45
Furlan E. et al., 2007, ApJ, 664, 1176
Gáspár A., Psaltis D., Rieke G. H., Özel F., 2012, ApJ, 754, 74
Gáspár A., Rieke G. H., Balog Z., 2013, ApJ, 768, 25
Greaves J. S., Wyatt M. C., 2010, MNRAS, 404, 1944
Gregorio-Hetem J., Lepine J. R. D., Quast G. R., Torres C. A. O., de La Reza R., 1992, AJ, 103, 549
Hinz P. M., 2009, in Usuda T., Tamura M., Ishii M., eds, AIP Conf. Ser. Vol. 1158, Exoplanets and Disks: Their Formation and Diversity. Am. Inst. Phys., New York, p. 313
Høg E. et al., 2000, A&A, 355, L27
Holmberg J., Nordström B., Andersen J., 2009, A&A, 501, 941
Honda M. et al., 2004, ApJ, 610, L49
Houck J. R. et al., 2004, ApJS, 154, 18
Ishihara D. et al., 2010, A&A, 514, A1
Jackson A. P., Wyatt M. C., 2012, MNRAS, 425, 657
Jarrett T. H. et al., 2011, ApJ, 735, 112
Kains N., Wyatt M. C., Greaves J. S., 2011, MNRAS, 414, 2486
Kasting J. F., Whitmire D. P., Reynolds R. T., 1993, Icarus, 101, 108
Kennedy G. M., Wyatt M. C., 2011, MNRAS, 412, 2137
Kennedy G. M., Wyatt M. C., 2012, MNRAS, 426, 91
Kennedy G. M. et al., 2012a, MNRAS, 421, 2264
Kennedy G. M., Wyatt M. C., Sibthorpe B., Phillips N. M., Matthews B. C., Greaves J. S., 2012b, MNRAS, 426, 2115
Kenyon S. J., Bromley B. C., 2004, ApJ, 602, L133
Kenyon S. J., Bromley B. C., 2005, AJ, 130, 269

Kopparapu R. K. et al., 2013, ApJ, 765, 131

Kresak L., 1980, in Halliday I., McIntosh B. A., eds, Proc. IAU Symp. 90, Solid Particles in the Solar System. Reidel, Dordrecht, p. 211

Lawler S. M. et al., 2009, ApJ, 705, 89

Lebouteiller V., Barry D. J., Spoon H. W. W., Bernard-Salas J., Sloan G. C., Houck J. R., Weedman D. W., 2011, ApJS, 196, 8

Levison H. F., Duncan M. J., 1997, Icarus, 127, 13

Lisse C. M., Chen C. H., Wyatt M. C., Morlok A., 2008, ApJ, 673, 1106

Lisse C. M., Chen C. H., Wyatt M. C., Morlok A., Song I., Bryden G., Sheehan P., 2009, ApJ, 701, 2019

Lisse C. M. et al., 2012, ApJ, 747, 93

Liu W. M., Hinz P. M., Hoffmann W. F., Brusa G., Miller D., Kenworthy M. A., 2009, ApJ, 693, 1500

Löhne T., Krivov A. V., Rodmann J., 2008, ApJ, 673, 1123

Mamajek E. E., 2005, ApJ, 634, 1385

Meeus G., Bouwman J., Dominik C., Waters L. B. F. M., de Koter A., 2002, A&A, 392, 1039

Melis C., Zuckerman B., Rhee J. H., Song I., 2010, ApJ, 717, L57

Melis C., Zuckerman B., Rhee J. H., Song I., Murphy S. J., Bessell M. S., 2012, Nat, 487, 74

Meng H. Y. A., Rieke G. H., Su K. Y. L., Ivanov V. D., Vanzi L., Rujopakarn W., 2012, ApJ, 751, L17

Mennesson B., Serabyn E., Hanot C., Martin S. R., Liewer K., Mawet D., 2011, ApJ, 736, 14

Millan-Gabet R. et al., 2011, ApJ, 734, 67

Mookerjea B., Sandell G., Jarrett T. H., McMullin J. P., 2009, A&A, 507, 1485

Moór A. et al., 2011, ApJS, 193, 4

Morales F. Y., Rieke G. H., Werner M. W., Bryden G., Stapelfeldt K. R., Su K. Y. L., 2011, ApJ, 730, L29

Morales F. Y., Padgett D. L., Bryden G., Werner M. W., Furlan E., 2012, ApJ, 757, 7

Moshir M. et al., 1993, VizieR Online Data Catalog, 2156, 0

Nesvorný D., Jenniskens P., Levison H. F., Bottke W. F., Vokrouhlický D., Gounelle M., 2010, ApJ, 713, 816

Nordström B. et al., 2004, A&A, 418, 989

Olofsson J., Henning T., Nielbock M., Augereau J.-C., Juhàsz A., Oliveira I., Absil O., Tamanai A., 2013, A&A, 551, A134

Oudmaijer R. D., van der Veen W. E. C. J., Waters L. B. F. M., Trams N. R., Waelkens C., Engelsman E., 1992, A&AS, 96, 625

Perryman M. A. C., ESA, eds, 1997, ESA Special Publication, Vol. 1200, The HIPPARCOS and TYCHO Catalogues. ESA, Noordwijk

Petit J.-M., Morbidelli A., Chambers J., 2001, Icarus, 153, 338

Phillips N. M., Greaves J. S., Dent W. R. F., Matthews B. C., Holland W. S., Wyatt M. C., Sibthorpe B., 2010, MNRAS, 403, 1089

Pilbratt G. L. et al., 2010, A&A, 518, L1

Poglitsch A. et al., 2010, A&A, 518, L2

Rizzuto A. C., Ireland M. J., Robertson J. G., 2011, MNRAS, 416, 3108

Rizzuto A. C., Ireland M. J., Zucker D. B., 2012, MNRAS, 421, L97

Roberge A. et al., 2012, PASP, 124, 799

Sadakane K., Nishida M., 1986, PASP, 98, 685

Sheret I., Dent W. R. F., Wyatt M. C., 2004, MNRAS, 348, 1282

Siegler N., Muzerolle J., Young E. T., Rieke G. H., Mamajek E. E., Trilling D. E., Gorlova N., Su K. Y. L., 2007, ApJ, 654, 580

Sierchio J. M., Rieke G. H., Su K. Y. L., Plavchan P., Stauffer J. R., Gorlova N. I., 2010, ApJ, 712, 1421

Skrutskie M. F., Dutkevitch D., Strom S. E., Edwards S., Strom K. M., Shure M. A., 1990, AJ, 99, 1187

Smith R., Wyatt M. C., Dent W. R. F., 2008, A&A, 485, 897

Smith R., Wyatt M. C., Haniff C. A., 2012, MNRAS, 422, 2560

Song I., Zuckerman B., Weinberger A. J., Becklin E. E., 2005, Nat, 436, 363

Su K. Y. L., Rieke G. H., Stapelfeldt K. R., Smith P. S., Bryden G., Chen C. H., Trilling D. E., 2008, ApJ, 679, L125

Tetzlaff N., Neuhäuser R., Hohle M. M., 2011, MNRAS, 410, 190

Trilling D. E. et al., 2007, ApJ, 658, 1289

Trilling D. E. et al., 2008, ApJ, 674, 1086

Tsiganis K., Gomes R., Morbidelli A., Levison H. F., 2005, Nat, 435, 459

van Leeuwen F., 2007, A&A, 474, 653

Vieira S. L. A., Corradi W. J. B., Alencar S. H. P., Mendes L. T. S., Torres C. A. O., Quast G. R., Guimarães M. M., da Silva L., 2003, AJ, 126, 2971

Walker H. J., Wolstencroft R. D., 1988, PASP, 100, 1509

Walsh K. J., Morbidelli A., Raymond S. N., O'Brien D. P., Mandell A. M., 2011, Nat, 475, 206

Weinberger A. J., Becklin E. E., Song I., Zuckerman B., 2011, ApJ, 726, 72

Werner M. W. et al., 2004, ApJS, 154, 1

Wright C. O., Egan M. P., Kraemer K. E., Price S. D., 2003, AJ, 125, 359

Wright E. L. et al., 2010, AJ, 140, 1868

Wyatt M. C., 2008, ARA&A, 46, 339

Wyatt M. C., Greaves J. S., Dent W. R. F., Coulson I. M., 2005, ApJ, 620, 492

Wyatt M. C., Smith R., Greaves J. S., Beichman C. A., Bryden G., Lisse C. M., 2007a, ApJ, 658, 569

Wyatt M. C., Smith R., Su K. Y. L., Rieke G. H., Greaves J. S., Beichman C. A., Bryden G., 2007b, ApJ, 663, 365

Wyatt M. C. et al., 2012, MNRAS, 424, 1206

Yang H. et al., 2012, ApJ, 744, 121

Zuckerman B., Becklin E. E., 1993, ApJ, 406, L25

Zuckerman B., Forveille T., Kastner J. H., 1995, Nat, 373, 494

Zuckerman B., Fekel F. C., Williamson M. H., Henry G. W., Muno M. P., 2008, ApJ, 688, 1345

APPENDIX A: NOTES ON INDIVIDUAL SOURCES

Notes for the 96 sources identified as having 12 μm excesses based on the criteria outlined in Sections 2 and 3. The 25 warm dust systems are shown in bold face. Stars noted as bright and very bright are those where saturation in W1 becomes an issue, meaning flux densities greater than ~1–10 Jy at 3 μm.

(1) HIP 999 (LN Peg). RS CVn. W3 excess not significant.

(2) HIP 3333 (NLTT 2305). Spectacularly aligned with a dust lane in Andromeda (M 31). Excess very likely not real.

(3) HIP 8920 (**BD+20 307**). Well-known warm dust source (Song et al. 2005; Weinberger et al. 2011). Dust temperature is about 400 K.

(4) HIP 9269 (HD 12051). No excess. *W*1 underestimated and *WISE* catalogue shows significant variability. May be affected by bright nearby source (BD+32 361).

(5) HIP 11696 (**HD 15407A**). Known warm dust source from AKARI (Melis et al. 2010; Fujiwara et al. 2012a,b). Age from Holmberg et al (2009) is 2.1 Gyr, but Melis et al (2010) show that Lithium absorption and kinematics argue that HD 15407AB is a member of the AB Doradus moving group and has an age of about 80 Myr. Dust temperature is about 550 K.

(6) HIP 14479 (**HD 19257**). Bright star nearby (IRAS 03038+3018), but at 1.6 arcmin is well separated enough for reliable *WISE* extraction. *WISE* images clean so excess likely robust. Likely missed by *IRAS* due to being masked by the bright (0.9 Jy at 12 μm and 0.4 Jy at 25 μm) nearby source. Dust temperature is 253 K. Spectral type is A5 from SIMBAD, but we find an effective temperature of 7485 K, closer to a late-A or early F-type.

(7) HIP 15244 (HD 20395). W3 excess not significant.

(8) HIP 17091 (**HD 22680**). Known 24 μm excess source in the Pleiades (Sierchio et al. 2010). Dust temperature is 202 K.

(9) HIP 17401 (**HD 23157**). Pleiades member (Sierchio et al. 2010). Clean detection in *WISE* images. No nearby sources. Excess appears robust. Dust temperature is 184 K.

(10) HIP 17657 (**HD 23586**). Clean detection in *WISE* images. No nearby sources. Excess appears robust. Dust temperature is 285 K.

(11) HIP 17827 (HD 23623). W3 excess not significant.

(12) HIP 20612 (CPD-77 172B): About 10 arcsec from the primary HIP 20610 (HD 29058). No excess; high $W1 - W3$ caused by low $W1$ measurement (which is also marked as variable in the catalogue). Significant excess at *IRAS* 12 μm not confirmed by *WISE*.

(13) HIP 21619 (HD 29364). Binary, excess caused by unreliable $W1$ measurement.

(14) HIP 22449 (HD 30652). Very bright, $W1$ unreliable and underestimated. No excess.

(15) HIP 22531 (HD 31203). Binary but only single *WISE* source extracted. Significant $W3$ variability. Excess probably not real.

(16) HIP 22563 (HD 31532). W1 underestimated, no excess.

(17) HIP 23835 (HD 32923). Very bright, $W1$ unreliable and underestimated. No excess.

(18) HIP 24065 (HD 33269). W1 underestimated, no excess.

(19) HIP 26460 (HD 37495). Very bright, $W1$ unreliable and underestimated. No excess.

(20) HIP 26525 (HD 245710). About 1 arcmin from the extremely bright variable M7 giant GP Tau (HD 37291). In addition, the *WISE W3* photometry is marked as variable. Very likely that the excess is not real and the result of proximity to GP Tau.

(21) HIP 26756 (HD 37805). *WISE* images show very high background because this star lies in the L1630 molecular cloud in Orion (called MIR-31 by Mookerjea et al. 2009). Despite their conclusion that the emission was photospheric, their Multiband Imaging Photometer for Spitzer (MIPS) 24 μm photometry has an excess of $R_{24} \approx 4-5$. However, inspection of the images suggests that the MIPS excess is for the same reason as the excess seen in W4; the bright background.

(22) HIP 27284 (HD 38589). Very red bright object nearby in *WISE* images. Also detection in *IRAS* at 60 μm. Excess unlikely to be related to the star in question.

(23) HIP 28415 (HD 233190). Excess caused by halo from nearby bright star V442 Aur (HD 39864).

(24) HIP 30399 (HD 44582). *WISE* images show high background level, excess probably not real.

(25) HIP 30953 (HD 46273). $W3$ excess due to saturated $W1$ and not real. Excess reported in Trilling et al. (2007) at 70 μm, but this was only 2.7σ significant (i.e. may not be real either). Perhaps worth follow up observations to check.

(26) HIP 31160 (HD 47149). No excess. $W1$ underestimated, perhaps due to nearby source (BD+12 1221).

(27) HIP 32362 (HD 48737). No excess. Poor photospheric prediction due to saturated 2MASS photometry and unusable $W1 - 2$ photometry.

(28) HIP 35069 (HD 55128). W1 underestimated, no excess.

(29) HIP 35564 (WDS J07204-5219AB). Binary. Two *WISE* sources extracted so $W1$ measurement uncertain, the reason for a $W1 - W3$ excess, which the SED fitting shows is unlikely to be real.

(30) HIP 41319 (HD 71030). W1 underestimated, no excess.

(31) HIP 41389 (HD 71152). No excess. SED fitting shows that $W1$ is underestimated.

(32) HIP 42173 (HD 72946). Two *WISE* sources extracted so $W1$ measurement uncertain, the reason for a $W1 - W3$ excess, which the SED fitting shows is unlikely to be real.

(33) HIP 47605 (HD 83804). W1 underestimated, no excess.

(34) HIP 51459 (HD 90839).Very bright, W1 unreliable and underestimated. No excess.

(35) HIP 53484 (**HD 94893**). Excess appears real, dust temperature is 151 K. Mamajek (2005) noted this star in looking for new members of the TWA, but rejected it due to a large distance (97 pc) and ∼15° distance from the association centroid. Possible presence

of an excess suggests that membership of LCC should be considered.

(36) HIP 54155 (HD 96064). Binary for which only a single source was extracted. Significant $W3$ variability indicated by catalogue, so excess unlikely to be real.

(37) HIP 54745 (HD 97334). W1 underestimated, no excess.

(38) HIP 55505 (**HD 98800**). Well-known warm excess source in TWA (e.g. Walker & Wolstencroft 1988; Zuckerman & Becklin 1993). Age is about 8 Myr. Sometimes classed as a disc in 'transition' between the protoplanetary and debris disc phases (Furlan et al. 2007), with the argument perhaps strengthened due to the recent detection of H_2 (Yang et al. 2012). Dust temperature is 168 K.

(39) HIP 56354 (**HD 100453**). Well-known isolated Herbig Ae star (e.g. Meeus et al. 2002).

(40) HIP 56809 (HD 101177). Binary but only single *WISE* source extracted. Significant $W3$ variability. Excess probably not real.

(41) HIP 58220 (**HD 103703**). Member of Scorpius–Centaurus in LCC (de Zeeuw et al. 1999). The age is therefore about 17 Myr. With no evidence for significant far-IR emission (Chen et al. 2011), HIP 58220 can be considered a 12 μm excess system with a dust temperature of 264 K.

(42) HIP 58351 (HD 103941). SIMBAD spectral type is F2III and listed as a δ Del giant. SED fitting finds $T_{eff} = 5900$ K but $L_\star = 6 L_\odot$, suggesting that this star is not a true dwarf. We therefore do not consider it as a warm dust source for our purposes here.

(43) HIP 59431 (HD 105963B). W1 underestimated, no excess.

(44) HIP 59693 (**HD 106389**). Member of Scorpius–Centaurus in LCC (de Zeeuw et al. 1999). The age is therefore about 17 Myr. With no evidence for significant far-IR emission (Chen et al. 2011), HIP 59693 can be considered a 12 μm excess system with a dust temperature of 291 K.

(45) HIP 60197 (BD+27 2115). Binary but only single *WISE* source extracted. Significant $W3$ variability. Excess probably not real.

(46) HIP 61049 (**HD 108857**). Member of Scorpius–Centaurus in LCC (de Zeeuw et al. 1999). The age is therefore about 17 Myr. With no evidence for significant far-IR emission (Chen et al. 2011), HIP 61049 can be considered a 12 μm excess system with a dust temperature of 220 K.

(47) HIP 61174 (η Crv, HD 109085). Well-known warm dust source. However, the *WISE* excess is not significant and arises here because of W1 underestimation due to the star being very bright. Not included in our luminosity function.

(48) HIP 62472 (HD 11261). Binary but only single *WISE* source extracted. Significant $W3$ variability. Excess probably not real.

(49) HIP 63439 (HD 112810). Member of Scorpius–Centaurus in LCC (de Zeeuw et al. 1999). The age is therefore about 17 Myr. Chen et al. (2011) find a large 70 μm flux, suggesting that the 12 μm excess is probably the Wien side of cooler (67K) emission. The detailed SED model finds that the 12 μm excess is only 2.4σ significant, so this source is not considered as a true warm dust source.

(50) HIP 63975 (**HD 113766A**). Well-known warm dust source in LCC (de Zeeuw et al. 1999; Oudmaijer et al. 1992; Lisse et al. 2008). The age is therefore about 17 Myr. The excess appears around the primary star in this binary system, the companion is about 160 au distant so too distant to affect the warm dust unless the eccentricity is very high (see Smith et al. 2012).

(51) HIP 64184 (HD 114082). Member of Scorpius–Centaurus in LCC (de Zeeuw et al. 1999). The age is therefore about 17 Myr. Chen et al. (2011) find a large 70 μm flux, suggesting that the

12 μm excess is probably the Wien side of cooler (110 K) emission. The detailed SED model finds that the 12 μm excess is only 2σ significant, so this source is not considered as a true warm dust source.

(52) HIP 64241 (HD 114378J). Very bright, W1 unreliable and underestimated. No excess.

(53) HIP 64532 (HD 115043). No excess. SED fitting shows that *W1* is underestimated. No excess found from *Spitzer* IRS (Lawler et al. 2009).

(54) HIP 64837 (**HD 115371**). Proposed as a member of Scorpius–Centaurus in LCC by Rizzuto et al. (2011, 2012) with 69 per cent probability. Hence, age is likely 17 Myr. Disc temperature is 238 K.

(55) HIP 64995 (HD 115600). Member of Scorpius–Centaurus in LCC (de Zeeuw et al. 1999). The age is therefore about 17 Myr. Chen et al. (2005) find a large 70 μm flux, suggesting that the 12 μm excess is probably the Wien side of cooler (120 K) emission. The detailed SED model finds that the 12 μm excess is only 1.4σ significant, so this source is not considered a true warm dust source.

(56) HIP 65875 (HD 117214). Member of Scorpius–Centaurus in LCC (de Zeeuw et al. 1999). The age is therefore about 17 Myr. Chen et al. (2011) find a large 70 μm flux, suggesting that the 12 μm excess is probably the Wien side of cooler (110 K) emission. The detailed SED model finds that the 12 μm excess is only 2σ significant, so this source is not considered a true warm dust source.

(57) HIP 67497 (HD 120326). Member of Scorpius–Centaurus in LCC (de Zeeuw et al. 1999). The age is therefore about 17 Myr. Chen et al. (2011) find a large 70 μm flux, suggesting that the 12 μm excess is probably the Wien side of cooler (105 K) emission. The detailed SED model finds that the 12 μm excess is only 1σ significant, so this source is not considered a true warm dust source.

(58) HIP 67970 (HD 121189). Member of Scorpius–Centaurus in UCL (de Zeeuw et al. 1999). The age is therefore about 15 Myr. Excess found at 24 μm by Chen et al. (2011), but no longer wavelength detection. *WISE* 12 μm excess is only 2.5σ significant, so this source is not considered a true warm dust source.

(59) HIP 69953 (HD 125038). *WISE* images show filamentary structure, excess unlikely to be real.

(60) HIP 71957 (HD 129502). Very bright nearby star, SED fit shows excess unlikely to be real due to *W1* saturation.

(61) HIP 73241 (HD 131923). No excess. SED fitting shows *W1* is underestimated and *WISE* catalogue shows significant variability.

(62) HIP 73990 (**HD 133803**). Member of Scorpius–Centaurus in UCL (de Zeeuw et al. 1999). The age is therefore about 15 Myr. Excess found at 24 μm by Chen et al. (2012), but no longer wavelength detection. Dust temperature is 177 K.

(63) HIP 77190 (HD 327427): *WISE* images suggest moderate nearby background level, and that W4 excess most likely not real. W3 excess questionable (and only 3.3σ) so not considered a true warm dust source.

(64) HIP 77545 (HD 141441). *WISE* images show high background levels so excess most likely not real.

(65) HIP 78996 (**HD 144587**). Member of Scorpius–Centaurus in US (de Zeeuw et al. 1999). The age is therefore about 11 Myr. Excess found at 24 μm by Carpenter et al. (2009), but no longer wavelength detection. Dust temperature is 223 K.

(66) HIP 79054 (HD 144729). W3 excess not significant.

(67) HIP 79288 (**HD 145263**). Member of Scorpius–Centaurus in US (de Zeeuw et al. 1999). The age is therefore about 11 Myr. Excess found at 24 μm by Chen et al. (2012), but no longer wavelength detection. Dust temperature is 241 K.

(68) HIP 79383 (**HD 145504**). Proposed as a member of Scorpius–Centaurus in US by Rizzuto et al. (2011) with 74 per cent probability. Hence, age is likely 17 Myr. Disc temperature is 206 K.

(69) HIP 79476 (**HD 145718**). Member of Scorpius–Centaurus in US (de Zeeuw et al. 1999). The age is therefore about 11 Myr. Known Herbig Ae star (Vieira et al. 2003; Carmona et al. 2010).

(70) HIP 79607 (HD 146361). Multiple system. Very bright, *W1* underestimated and excess unlikely.

(71) HIP 79977 (HD 146897). Member of Scorpius–Centaurus in US (de Zeeuw et al. 1999). The age is therefore about 11 Myr. Chen et al. (2011) find a large 70 μm flux, suggesting that the 12 μm excess is probably the Wien side of cooler (89 K) emission. The detailed SED model finds that the 12 μm excess is just below 3σ significant, so this source is not considered a true warm dust source.

(72) HIP 80170 (HD 147547). Very bright, SED fitting shows that *W1* is underestimated and excess unlikely.

(73) HIP 80759 (HD 148371). Excess in SED appears reliable. *WISE* images show possible contamination due to filamentary background at both W3 and W4, though whether the excess is caused by this is hard to tell. The W3 excess is 3.6σ, so the background contribution would not need to be large to cause the excess to be significant. Therefore, we do not include this source as a warm dust candidate.

(74) HIP 81870 (**HD 150697**). Noted as a possible warm dust source from *IRAS* photometry by Fajardo-Acosta et al. (2000), but with the caution that the star lies on the edge of the ρ Oph star-forming region. With a distance of 133 pc, it may in fact be a young star associated with ρ Oph, but was assigned an age of 3.2 Gyr by Holmberg et al. (2009). We find that the *IRAS* 12 μm excess is 2.98σ significant and that the W3 images appear clean, so the excess appears reliable. Dust temperature is 234 K.

(75) HIP 83006 (HD 153525). Bright star, W1 underestimated, no excess.

(76) HIP 83301 (HD 153592). Near edge of region with no *W3* coverage, image has major artefacts so excess very unlikely to be real.

(77) HIP 83877 (**HD 154593**). *WISE* images appear reasonably clean though the source is not very bright. Very bright carbon star to the North (IRAS 17050−4642) does not appear to affect the images at the target position. That an excess is seen in both W3 and W4 suggests that it is real, with a dust temperature of 285 K.

(78) HIP 84720 (HD 156274). Very bright, SED fitting shows that *W1* is underestimated and excess unlikely.

(79) HIP 85340 (HD 157792). Bright star, W1 underestimated, no excess.

(80) HIP 86596 (HD 161157). Bright star, W1 underestimated, no excess.

(81) HIP 86853 (**HD 160959**). Excess found by Rizzuto et al. (2012) and UCL membership assigned 50 per cent probability based on this excess. Disc temperature is 205 K.

(82) HIP 87368 (HD 162186). Has a 3.8σ *W3* excess, but is very near the Galactic centre ($<5°$) so in a high background region and probably not real. Very bright *IRAS* 60 and 100 μm detections, and a *ROSAT* X-ray detection 33 arcsec to the south-east (1RXS J175106.2−321836), which is unlikely to be associated given the 10 arcsec position uncertainty. The *IRAS* excess may be associated with the X-ray source.

(83) HIP 88683 (HD165269). No excess. SED fitting shows that *W1* is underestimated and *WISE* catalogue shows significant variability.

(84) HIP 88692 (*HD 165439*). Excess appears reliable. Age of 11 Myr derived by Tetzlaff et al. (2011).

(85) HIP 89046 (**HD 166191**). Large far-IR excess from AKARI and *IRAS* may be associated with nearby red source. Alternatively, far-IR emission could be associated with HIP 89046 and it harbours a previously unknown transitional protoplanetary disc. Preliminary conclusion from *Herschel* PACS observations favours the protoplanetary disc interpretation.

(86) HIP 91242 (HD 171452). *WISE* images appear clean and significant excess at W4. W3 excess only 2σ significant so not considered a warm dust source here.

(87) HIP 93940 (HD 178332). No excess. *W1* underestimated and *WISE* catalogue shows significant variability.

(88) HIP 100217 (HD 193632). Bright star, W1 underestimated, no excess.

(89) HIP 100464 (*HD 194931*). Excess appears reliable in *WISE* images. Dust temperature is 188 K.

(90) HIP 107556 (HD 207098). Bright star, *W1* saturated and *W3* excess not real.

(91) HIP 108431 (HD 208450). Bright star, W1 underestimated, no excess.

(92) HIP 108456 (HD 209942): About 13 arcsec from the RS CVn secondary V376 Cep (HD 209943). Both stars have very similar K_s magnitudes of 5.6, meaning that if the *WISEW3* photometry covers the pair (as suggested by the catalogue) it would show a flux ratio of about 2. The *W3* flux ratio is 2.7 (and 2 for *IRAS* 12 μm), but the *WISE* photometry is also variable in $W1 - 3$, suggesting that the excess is spurious.

(93) HIP 110355 (HD 211729). Bright star, W1 underestimated, no excess.

(94) HIP 110785 (HD 212754). Bright star, W1 underestimated, no excess.

(95) HIP 111278 (HD 213617). Significant 60 μm excess from *IRAS* and 70 μm excess from *Spitzer* (Moór et al. 2011), *WISE* 12 μm excess not significant.

(96) HIP 114944 (EZ Peg). W3 excess not significant.

APPENDIX B: SAMPLE AGE DISTRIBUTION

While stars of a given spectral type may reasonably be assumed to have random main-sequence ages, our sample spans a sufficiently wide range of spectral types that the main-sequence lifetimes τ_{MS} vary significantly. Because our stars are selected based on their Tycho-2 $B_T - V_T$ colour, to derive the age distribution we want a relation between this colour and τ_{MS}.

About 10 000 of our 24 174 stars actually have ages derived by The Geneva–Copenhagen survey of the solar neighbourhood (Nordström et al. 2004; Holmberg et al. 2009). The ages are derived using isochrones, and therefore have the weakness that stars not sufficiently evolved from the zero-age main sequence cannot be assigned ages. Indeed, the authors state 'that the true age distribution of the full sample cannot be derived directly from the catalogue; careful simulation of the biases operating on the selection of the stars and their age determination will be needed to obtain meaningful results in investigations of this type.' Despite this limitation, however, the catalogue does provide a distribution of ages as a function of colour, shown in Fig. B1, which can be used to verify an empirical relation between τ_{MS} and $B_T - V_T$.

We first plot absolute luminosities as derived by SED fitting against colour for main-sequence stars from the UNS sample (Phillips et al. 2010) in Fig. B2. The correlation in this HR diagram is reasonably well described as $L_\star \propto 10^{-1.5(B_T - V_T)}$. This relation,
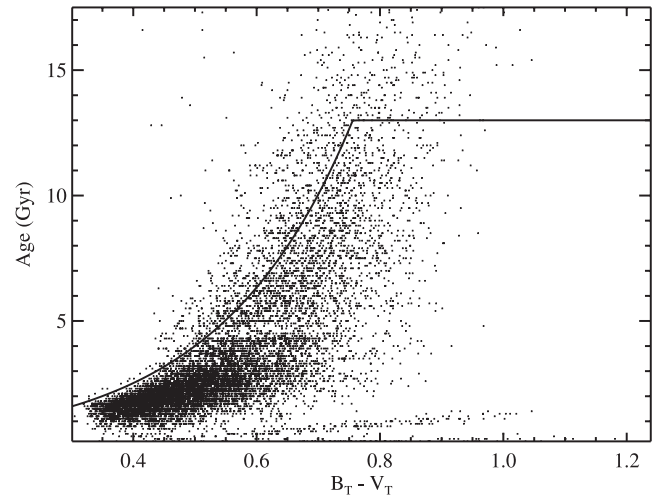
Figure B1. Age versus Tycho-2 colour for 10 593 stars in the Geneva–Copenhagen catalogue with age estimates. The line shows an empirical estimate for the main-sequence lifetime of $\tau_{MS} = 0.4 \times 10^{(B_T - V_T)/0.5}$ Gyr, where ages are also restricted to be less than 13 Gyr.
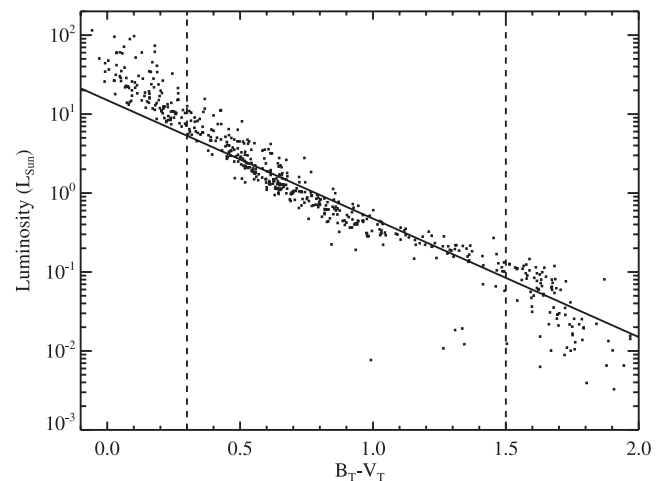
Figure B2. HR diagram for stars from the UNS sample, where stellar luminosities have been derived from SED fitting. The solid line is $L_\star = 15 \times 10^{-1.5(B_T - V_T)}$, and the dashed lines show the $B_T - V_T$ colour range of our sample.

combined with $\tau_{MS} \propto M_\star/L_\star$ (i.e. assuming all mass is turned into energy) and $L_\star \propto M_\star^{3.5}$ yields $\tau_{MS} \propto 10^{B_T - V_T}$. This dependence is only approximate however. Using it as a starting point, with some experimentation we found that

$$\tau_{MS} = 0.4 \times 10^{(B_T - V_T)/0.5} \text{ Gyr} \qquad (B1)$$

provides a reasonable match to the maximum ages for early-types in Fig. B1, while giving an age of 9 Gyr at $B_T - V_T = 0.68$, corresponding approximately to the Sun. We add a further restriction that ages must be less than 13 Gyr.

To derive the age distribution of our sample now requires converting the known distribution of colours. This conversion is done by setting up a series of colour bins, and selecting ages randomly between zero and τ_{MS} for the stars in each bin. This process results in the age distribution for our sample shown in Fig. 2.

To generate this distribution numerically we make use of a fourth-order polynomial fit to the histogram, with coefficients

of 0.171 124, −0.052 8395, 0.006 862 27, −0.000 410 586 and 9.293 93e-06. We generate a random age in the desired range, and another random number between 0 and 0.1035. If the second random number is lower than the polynomial function evaluated for that age, or if the polynomial is greater than 0.1035, we keep the age. This process is repeated until the desired number of ages is acquired.

Our analysis has been done with both a naive uniform distribution of ages between 0 and 10 Gyr and the more detailed distribution derived above, and our conclusions are the same for either distribution.

APPENDIX C: SEDS FOR 25 WARM DUST CANDIDATES/SYSTEMS
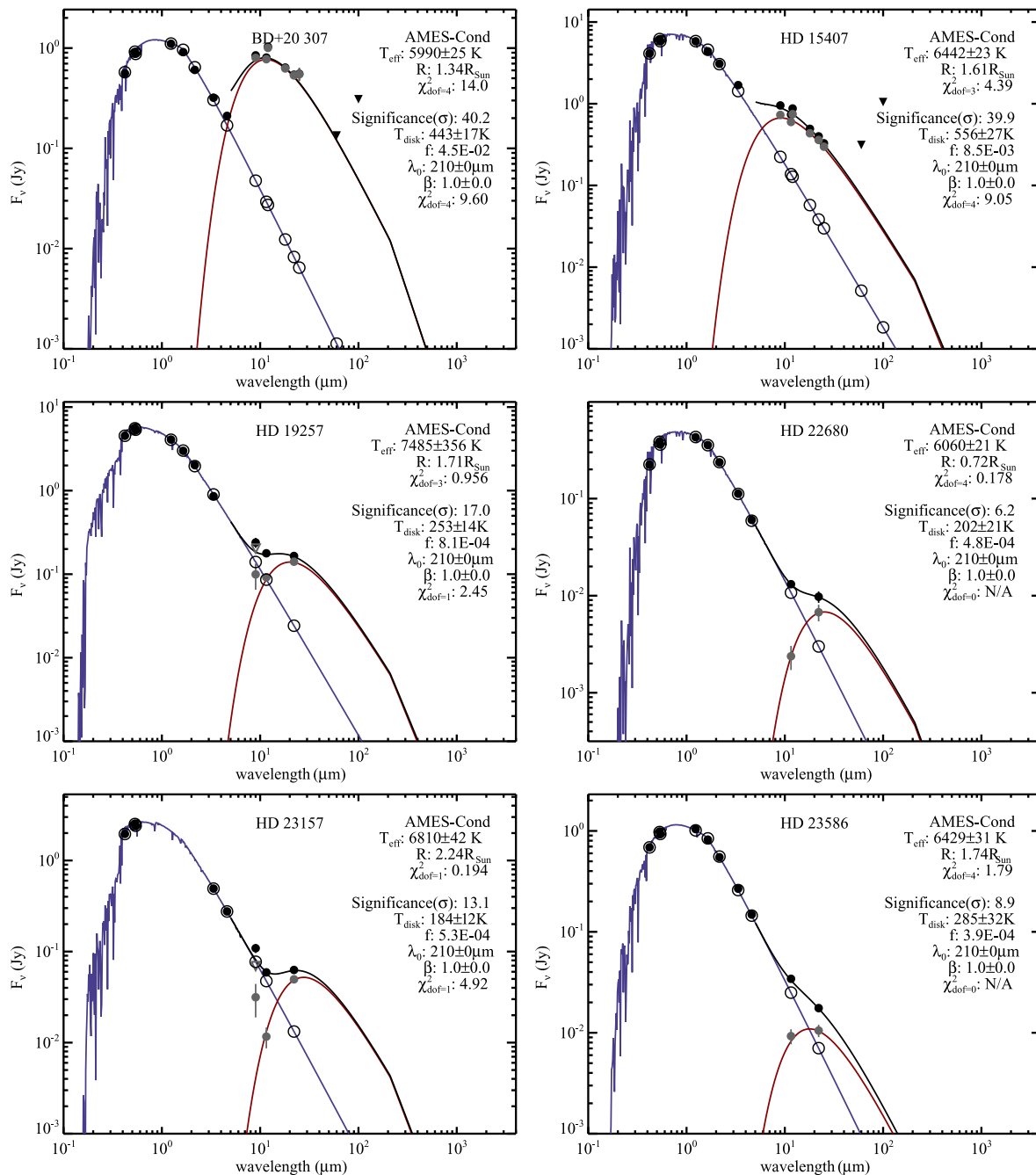
Figure C1. SED modelling for the 25 candidate warm dust systems from Table 1 (i.e. including the three that are excluded from the final list of 22). Each panel shows PHOENIX stellar (blue), blackbody disc (red) and star+disc spectra (black). Photometry is shown as filled dots and photospheric model fluxes at these wavelengths as open circles. Star-subtracted (i.e. disc) fluxes are shown as grey filled dots. Upper limits are shown as downward pointing triangles. The legend for each panel shows the parameters of the stellar and disc models. Modified blackbody parameters of $\lambda_0 = 210$ μm and $\beta = 1$ have been assumed (Wyatt 2008).
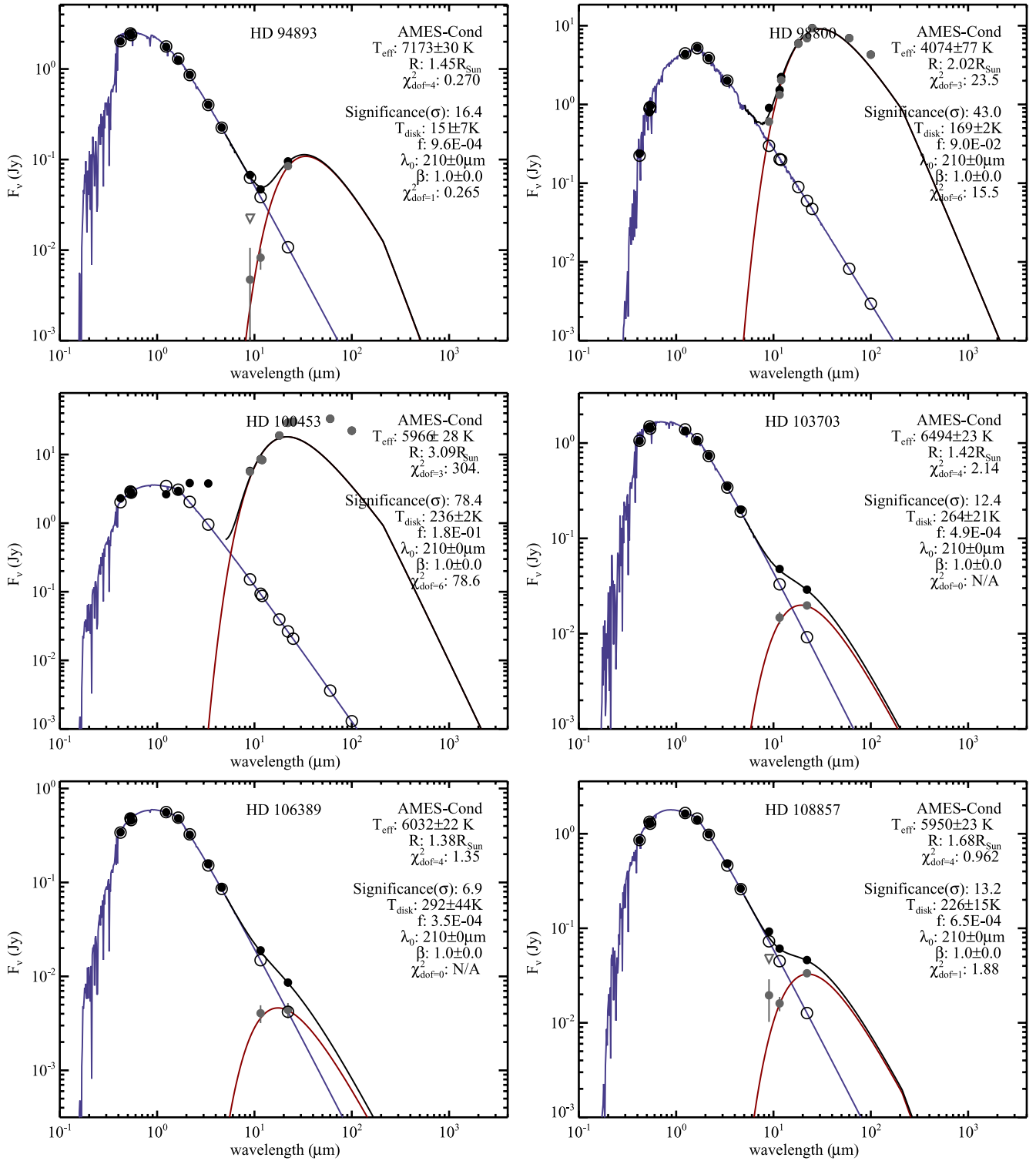
Figure C2. 25 warm dust systems continued from Fig. C1.

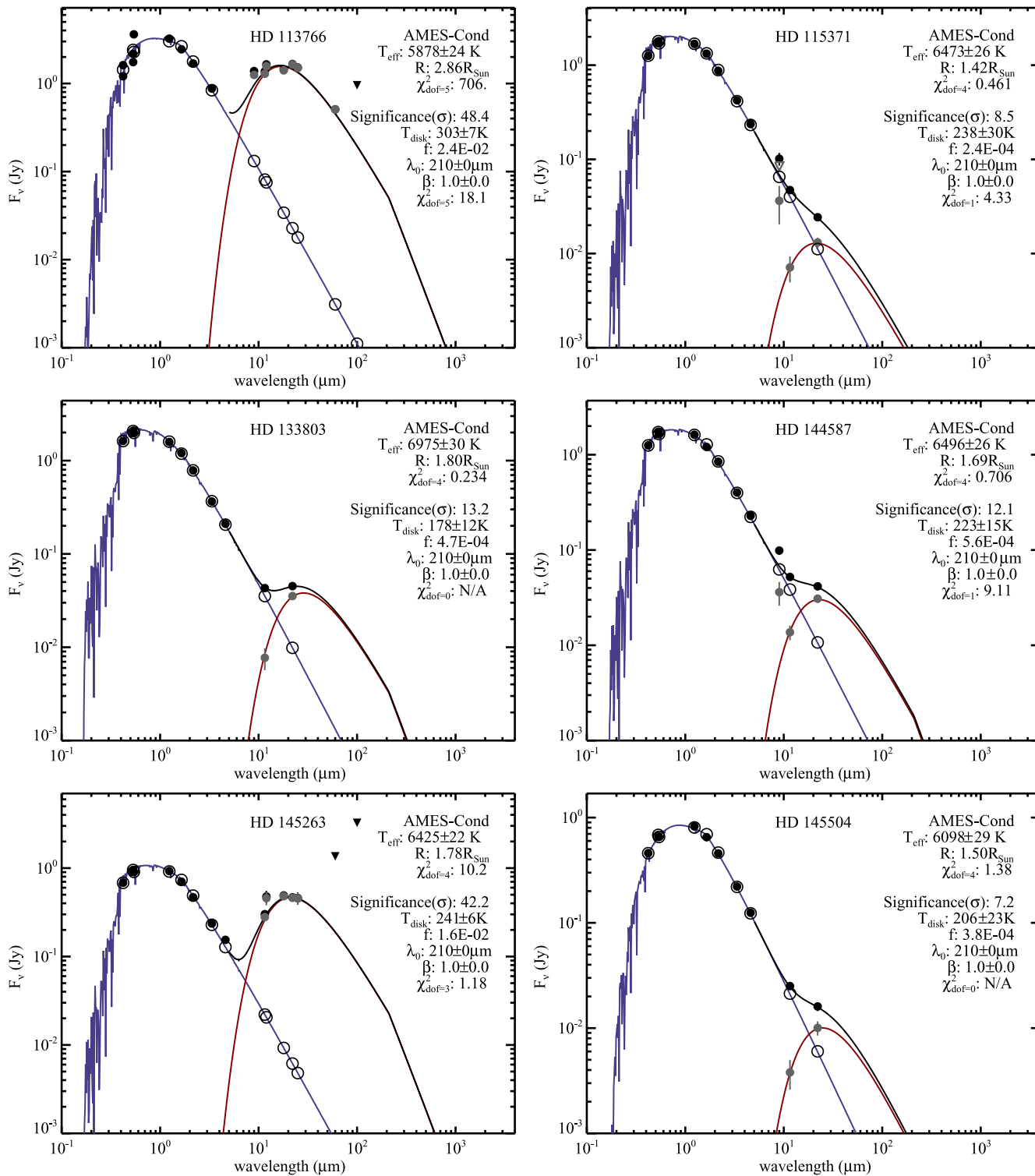**Figure C3.** 25 warm dust systems continued from Fig. C2.
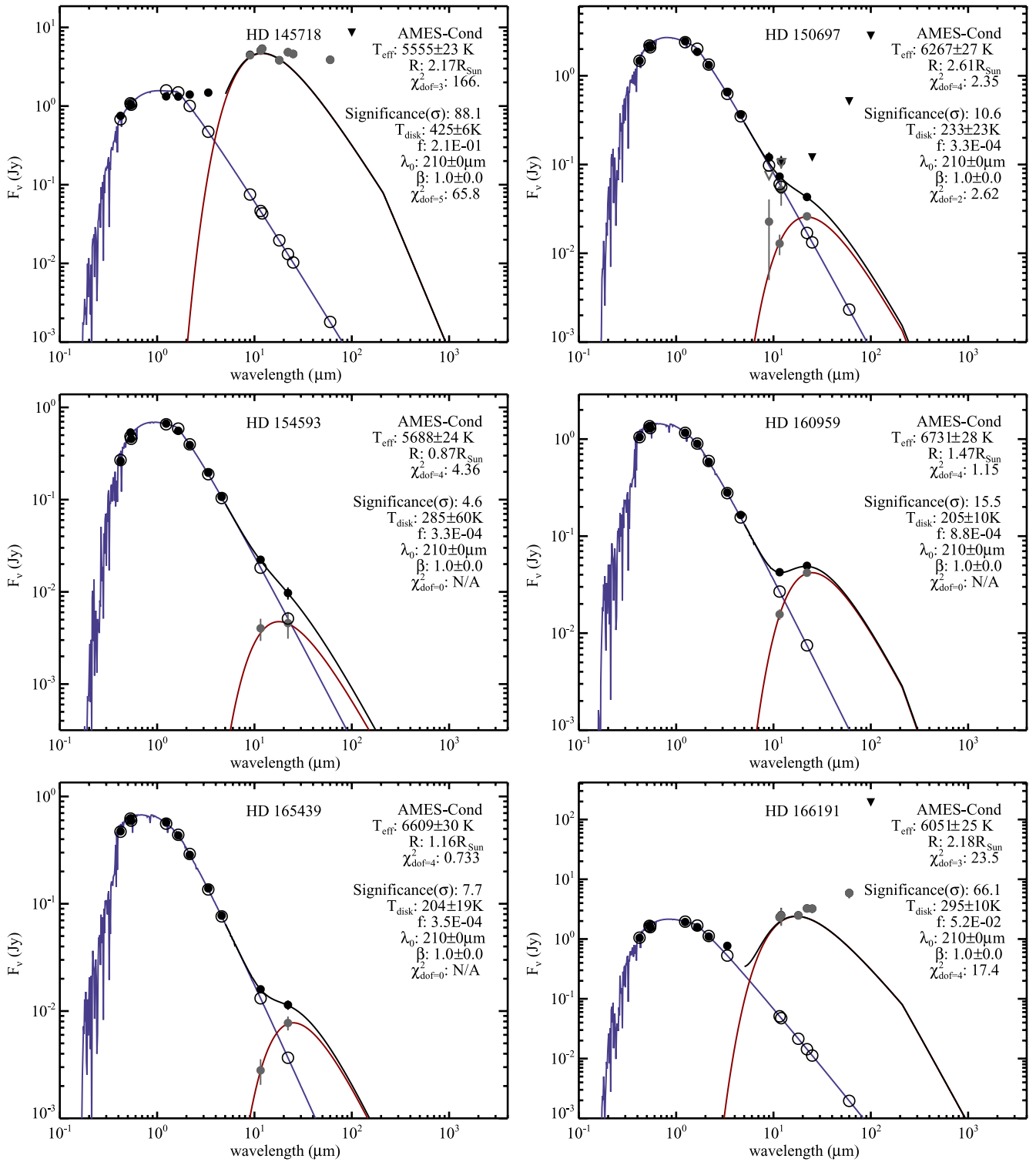
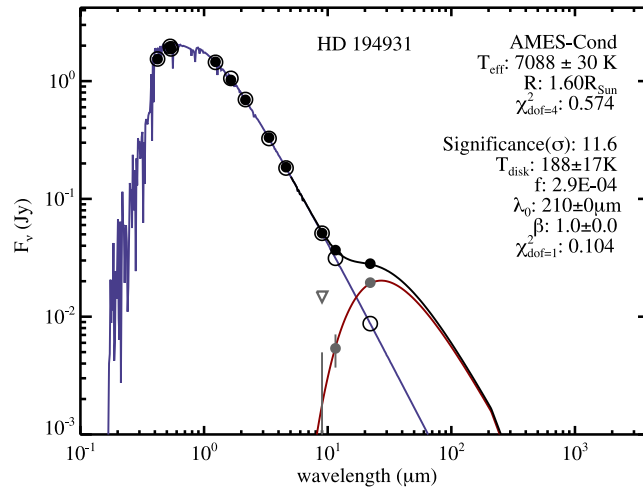**Figure C4.** 25 warm dust systems continued from Fig. C3.

Figure C5. 25 warm dust systems continued from Fig. C4.

This paper has been typeset from a TEX/LATEX file prepared by the author.